Title

Hypothalamic Pomc Neurons Innervate the Spinal Cord and Modulate the Excitability of Premotor Circuits.

Journal

Current biology : CB, 30(23)

ISSN

0960-9822

Authors

Reinoß, Philip
Ciglieri, Elisa
Minére, Marielle
et al.

Publication Date

2020-12-01

DOI

10.1016/j.cub.2020.08.103

Peer reviewed

HHS Public Access

Author manuscript

Curr Biol. Author manuscript; available in PMC 2022 February 16.

Published in final edited form as:

Curr Biol. 2020 December 07; 30(23): 4579–4593.e7. doi:10.1016/j.cub.2020.08.103.

Hypothalamic Pomc neurons innervate the spinal cord and modulate the excitability of premotor circuits

Philip Reinoß[1], **Elisa Ciglieri**[2,3], **Marielle Minere**[2,3], **Stephan Bremser**[1,2], **Andreas Klein**[1], **Heiko Löhr**[1], **Patrick M. Fuller**[4], **Ansgar Büschges**[1], **Peter Kloppenburg**[1,5], **Henning Fenselau**[2,3,5,*], **Matthias Hammerschmidt**[1,5,6,*,#]

[1] Institute for Zoology, University of Cologne, Zülpicher Straße 47b, 50674 Cologne, Germany

[2] Synaptic Transmission in Energy Homeostasis Group, Max Planck Institute for Metabolism Research, Gleueler Straße 50, 50931 Cologne, Germany

[3] Center for Endocrinology, Diabetes and Preventive Medicine (CEDP), University Hospital Cologne, Kerpener Straße 26, 50924 Cologne, Germany

[4] Department of Neurology, Program in Neuroscience, Beth Israel Deaconess Medical Center and Harvard Medical School, 330 Brookline Avenue, Boston, MA 02215, USA

[5] Cologne Excellence Cluster on Cellular Stress Responses in Aging-Associated Diseases, University of Cologne, Joseph-Stelzmann-Straße 26, 50931 Cologne, Germany

[6] Center for Molecular Medicine Cologne, University of Cologne, Robert-Koch-Straße 21, 50931 Cologne, Germany

Summary

Locomotion requires energy, yet animals need to increase locomotion in order to find and consume food in energy-deprived states. While such energy homeostatic coordination suggests brain origin, whether the central melanocortin 4 receptor (Mc4r) system directly modulates locomotion through motor circuits is unknown. Here, we report that hypothalamic Pomc neurons in zebrafish and mice have long-range projections into spinal cord regions harboring *Mc4r*-expressing V2a interneurons, crucial components of the premotor networks. Furthermore, in zebrafish, Mc4r activation decreases the excitability of spinal V2a neurons as well as swimming and foraging, while systemic or V2a neuron-specific blockage of Mc4r promotes locomotion. In contrast, in mice, electrophysiological recordings revealed that two-thirds of V2a neurons in lamina X are excited by the Mc4r agonist α-MSH, and acute inhibition of Mc4r signaling reduces locomotor activity. In addition, we found other Mc4r neurons in spinal lamina X that are inhibited by α-MSH, which is in line with previous studies in rodents where Mc4r agonists reduced locomotor activity. Collectively, our studies identify spinal V2a interneurons as evolutionary

[*] Authors for correspondence: HF: phone: +49-221-4726-217; fax: +49-221-4726-298; henning.fenselau@sf.mpg.de, MH: phone: +49-221-470 5665; fax: +49-221-470 5164; mhammers@uni-koeln.de.

Author Contributions

PR, HL, AB, and MH conceived, designed, performed, and analyzed the zebrafish experiments, EC, MM, AK, SB, PF, PK, and HF the mouse experiments. PR, HF, and MH wrote the manuscript with input from all authors.

[#]lead contact:

Declaration of Interests

The authors declare no competing interests.

conserved second-order neurons of the central Mc4r system, providing a direct anatomical and functional link between energy homeostasis and locomotor control systems. The net effects of this modulatory system on locomotor activity can vary between different vertebrate species and, possibly, even within one species. We discuss the biological sense of this phenomenon in light of the ambiguity of locomotion on energy balance and the different living conditions of the different species.

Keywords

Pomc; Agrp; Mc4r; neurocircuit; spinal cord; interneurons; energy homeostasis; locomotion; zebrafish; mouse

Introduction

In order to survive, animals need to balance their energy homeostasis in times of food in abundance and when energy supplies are rare [1]. Therefore, they need to control how much energy they should spend on finding energy resources because locomotion during foraging and hunting depletes their energy stores. The central Mc4r system plays a key role in controlling energy homeostasis [2]. It determines the energy state of the body by responding to hormones like leptin, insulin or ghrelin that circulate in the blood. Two cell populations with antagonistic functions build the core of the Mc4r system: Pro-opiomelanocortin (Pomc) and Agouti-related peptide (Agrp) neurons. Pomc and Agrp neurons are located in the arcuate nucleus of the hypothalamus (ARC), a conserved region among vertebrates and named nucleus lateralis tuberis in fish [3]. Activation of Pomc neurons promotes satiety and increases energy expenditure through release of the Pomc-derived neuropeptide α-MSH. In contrast, activation of Agrp neurons and the neuropeptide they release (Agrp) promote food intake and decrease energy expenditure [2]. α-MSH and Agrp act as agonist and antagonist, respectively, at the Mc4r transmembrane receptor. Consistent with the above, deficiency of Mc4r results in hyperphagia and early-onset obesity in mice [4] and in humans [5]. Given the action of α-MSH and Agrp on Mc4r, Mc4r-expressing neurons are the direct targets of Pomc and Agrp neurons. However, the identity of Mc4r-expressing neurons in many brain sites as well as the underlying neurocircuits remain largely elusive [6].

Previous studies in rodents have demonstrated that Mc4r signaling can have diverse impacts on locomotion. For example, intra-peritoneal injection of the Mc4r agonist Melanotan II (MTII) leads to long-term increases in locomotor activity in mice [7]. Consistent with this, administration of the Mc4r antagonist SHU9119 results in decreased activity in mice [8] and Mc4r-deficient mice are hypoactive even before they become obese [9]. These findings suggest that activation of the Mc4r, which reflects energy surplus, promotes physical activity. On the other hand, chemogenetic activation of Agrp neurons in absence of food as well as administration of SHU9119 increases locomotion, most likely representing foraging [10–12].

If these effects of the melanocortin system on locomotion are due to direct innervations of spinal premotor circuits by Pomc and/or Agrp neurons remains currently elusive. Interestingly, while Pomc projections to the intermediolateral cell column (IML) of the

thoracic spinal cord [13] and Mc4r-dependent control of presympathetic IML neurons have been suggested to regulate blood pressure and insulin levels [14], locomotor control is largely believed to be mediated indirectly via Mc4r-expressing neurons in the paraventricular nucleus of the hypothalamus (PVH) [15] or Mc3r-expressing neurons in the lateral hypothalamus (LHA) [16]. These brain sites, in turn, act via the mesencephalic locomotor region and its projections to the medial reticular formation in the lower brainstem to eventually regulate spinal circuits [15–17].

Premotor circuitries within the spinal cord have been rather thoroughly studied both in mouse and zebrafish [18–21]. During locomotion, central pattern generators (CPGs) generate the alternating activity pattern of the left and right side of the spinal cord and coordinate the activities in the different segments with each other. Spinal V2a interneurons marked by visual system homeobox 2 (Vsx2) are an intrinsic source of excitation for locomotor CPGs. They are crucial for the generation of locomotor rhythm, projecting to and activating motoneurons that in turn cause contractions of muscles along the trunk in fish or muscles in the legs in mice [22–29]. Ablation of these neurons in zebrafish larvae affects locomotor rhythm and intersegmental coordination, showing their importance in the CPG network [30].

Here, we identify spinal V2a as so far unrecognized direct second-order neurons of the Mc4r system both in zebrafish larvae and adult mice. We show that Mc4r agonists can modulate the excitability of these neurons in ways consistent with their effects on locomotor behaviors as reported here and elsewhere.

Results

Hypothalamic Pomca neurons innervate locomotor control regions of the zebrafish spinal cord

Using a recently published transgenic zebrafish line exclusively labeling Pomca neurons of the ARC [31], we found Pomca neurons to directly project into the hindbrain and to enter the spinal cord from a larval standard length (SL) of 8 mm onwards (corresponding to 12–15 days post fertilization (dpf); Figure S1A). At 10–11 mm SL (~25–30 dpf), Pomca fibers from the ARC (Figure S1B–B’’) had reached trunk levels (10^{th} somite; Figure 1A–C) while remaining strictly ipsilateral (Figure S1B’’’). As adults (30 mm SL; 10 months of age) they had reached precaudal regions up to the level of the dorsal fin. However, projections into more caudal spinal regions were not observed (data not shown). Notably, spinal Pomca projections displayed a differential dorso-ventral topology (Figure 1E) and were restricted to ventral regions of the spinal cord and the region surrounding the central canal, where locomotor circuits in vertebrates are primarily located. In contrast, no Pomca fibers were found in the dorsal spinal cord (Figure 1B, Supplemental Video 1). Motor circuits located in these ventral and central regions include V2a interneurons (Figure 1C) and motoneurons (Figure 1D) [28, 32], and indeed, 23% of CPG V2a interneurons labelled via a *vsx2:Gal4FF* transgene [33] were in a distance to Pomca axons below 5 μm (Figure 1B,C). Together, this demonstrates a preferential association of Pomc axons with ventral motor circuits but not with more dorsal ascending neurons. However, among V2a neurons themselves, contacts were not restricted to a specific dorsal or ventral subdivision (Figure 1E,F). Furthermore,

co-labeling of spinal Pomca axons, V2a neurons and the pre-synaptic marker SV2 revealed that synapses are present at the contact sites (Figure S1C).

Spinal zebrafish V2a neurons express *mc4r*

In light of the innervation of V2a neuron-harboring spinal regions by Pomca neurons, and the known function of V2a neurons during locomotion [22, 28, 29], we wondered whether V2a or motoneurons might be direct cellular targets of Pomc neurons. As a first step to test this notion, we studied whether they contain the Mc4r receptor. Via in situ hybridization, expression of *mc4r* was found in the same regions containing *vsx2*-positive V2a neurons or motoneurons (Figure 1G–I). Of the primary motoneurons, identified by their location and size, approximately one third displays *mc4r* expression (Figure 1J). Similarly, double labeling showed that 55% of the spinal V2a interneurons contain the Mc4r, constituting 17% of *mc4r*-positive cells in these spinal cord regions (Figure 1K,L).

In addition to the spinal cord, we also assessed Pomca projections and *mc4r* expression in hindbrain regions, which also harbor V2a neurons implicated in locomotor control [33]. Indeed, in hindbrains of 10 mm SL larvae, we observed Pomca projections in close contact to V2a neurons (Figure S1D). Furthermore, we found *mc4r* expression in hindbrain regions of SL10 and younger embryos that harbor V2a neurons (Figure S1E,F).

Pomc neurons in mice have long-range projections to spinal lamina X

In mice, effects of the Mc4r system on locomotion are supposed to be largely indirect, involving multiple intermediate brain sites (see Introduction). This, however, does not rule out the co-existence of an evolutionary conserved direct ARC to spinal cord projection, as revealed above for the zebrafish. To test this, we first analyzed spinal projections of ARC Pomc (ARC^{Pomc}) neurons by genetically labeling their axonal terminals. Adult *Pomc-Cre* mice were stereotaxically injected with a Cre-dependent adeno-associated virus (AAV) construct containing channelrhodopsin-2 (ChR2) fused to mCherry (AAV-DIO-ChR2-mCherry; Figure 2A). Expression of ChR2-mCherry was restricted to ARC^{Pomc} neurons as assessed by immunohistochemistry (Figure 2B). Analysis of brain sites known to be innervated by ARC^{Pomc} neurons [34], including the paraventricular nucleus of the hypothalamus (PVH), confirmed accurate labeling of ARC^{Pomc} projections (Figure S2A). As previously observed [13], we found that ARC^{Pomc} neurons innervate the intermediolateral cell column (IML) of the thoracic spinal cord (Figure 2C). Remarkably, in thoracic spinal cord sections we observed ARC^{Pomc} neuron axonal terminals surrounding the central canal region of Rexed's lamina X (Figure 2C). Notably, ARC^{Pomc} neuron innervation of spinal lamina X was not restricted to thoracic segments as found in zebrafish but could be observed in all segments of the cervical, lumbar, and sacral spinal cord (Figure S2B). Thus, ARC^{Pomc} neurons in mice send long-range projections to lamina X at all levels of the spinal cord.

Mouse Mc4r neurons in spinal lamina X express *Vsx2*

To determine whether ARC^{Pomc} neuron spinal projections engage *Mc4r*-expressing neurons, we next performed experiments using *Mc4r-t2a-Cre* knock-in mice that express Cre-recombinase under control of endogenous Mc4r regulatory elements [35]. In these

studies, *Mc4r-t2a-cre* mice were crossed to tdTomato reporter mice (Ai9; *Rosa26-CAG-loxSTOPlox-tdTomato*) [36]. In the resulting *Mc4r-t2a-cre::tdTomato* mice, spinal *Mc4r*-expressing neurons were visualized by expression of tdTomato (*Mc4r::tdTomato* neurons; Figure 2D). In thoracic spinal cord sections, *Mc4r::tdTomato* neurons were located in multiple sites, including the dorsal horn, the IML, the VH, as well as in lamina VII and lamina X (Figure 2D–F, Figure S2C–E). In the IML, we found that about half of *Mc4r::tdTomato* neurons were cholinergic neurons as assessed by expression of choline acetyltransferase (*Chat*) mRNA using in situ hybridization (RNAscope method; Figure S2C,E), confirming prior findings [14]. In the VH, approximately 40% of *Mc4r::tdTomato* neurons were also cholinergic, as determined by *Chat* mRNA expression (Figure 2F). Thus, *Mc4r-t2a-cre* targets multiple spinal thoracic neurons, including cholinergic preganglionic sympathetic neurons in the IML and cholinergic motor neurons in the VH, consistent with the findings in zebrafish (Figure 1J).

To test whether, as in larval zebrafish (Figure 1K,L), the population of thoracic *Mc4r*-expressing neurons in the mouse spinal cord also contains V2a interneurons, we performed in situ hybridization for *Vsx2* mRNA in *Mc4r-t2a-Cre::tdTomato* mice. We found that about two-thirds of *Mc4r::tdTomato* neurons in lamina X were positive for *Vsx2* (Figure 2D,E). In contrast, in lamina VII only approximately 20% of *Mc4r::tdTomato* neurons were *Vsx2*-positive (Figure S2C,D). These studies demonstrate that, in mice, the majority of *Mc4r*-expressing neurons in spinal lamina X are V2a interneurons.

Locomotion of zebrafish larvae is modulated by their feeding state and the melanocortin system

The direct innervation of spinal motor circuits by Pomc neurons suggests that they can modulate locomotion in adaptation to the energy state of the animals. To test this, we first studied fasted versus sated zebrafish larvae (8–9 mm SL, 20–25 dpf), which were obtained via 1–2 days of feeding with low (< 500/day and larva; fasted) or ad libitum (~20,000/day and larva; sated) amounts of paramecia, respectively (Figure 3A). As expected, fasted larvae displayed strongly increased transcript levels of the orexigenic peptide gene *agrp* (Figure S3A). Furthermore, fasted larvae, once supplied with paramecia, consumed more food when compared to sated larvae (Figure 3B and S3F). The increased food intake correlated with increased locomotor activity, which most likely involved prey hunting and feeding (Figure S3G). Fasted larvae kept in larger arenas [37, 38] also displayed moderately increased locomotion (approximately 11%) before paramecia were supplied, most likely representing foraging and exploratory activity (Figure 3D), although the difference to sated larvae became larger after addition of prey (approximately 42%). Analysis of swim bouts (see Figure 3C) revealed that bout frequency, bout speed and bout distance increased in fasted larvae in presence of food, whereas bout duration dropped slightly (Figure S4A). Smaller differences between fasted and sated larvae were observed in the absence of food (Figure S4D). Together, these findings indicate that the energy state of the larvae affects both their food search- and their food intake-dependent locomotion, which is consistent with recent reports on the effect of energy deprivation on interbout interval durations, and exploratory and hunting bout types [38].

To investigate if the Mc4r system is involved in mediating this behavior, we quantified locomotion during foraging and feeding with genetic or pharmacological interferences of Mc4r signaling. Gain of Mc4r signaling was obtained via the treatment of wild-type larvae with the Mc4r agonist MTII [39], or via genetic inactivation of its endogenous antagonist Agrp (see Figure S3C,D). In reverse, blockage of Mc4r signaling was obtained by treating larvae with the Mc4r antagonist SHU9119 [40], or by using formerly described *mc4r* null mutants [41]. The latter were raised under conditions not leading to size or weight differences compared to wild-type siblings (Figure S3E). Strikingly, in fasted larvae (which per se should have low Mc4r signaling), both pharmacological and genetic gain of Mc4r signaling led to decreased movement in presence as well as in absence of food (Figures 3E and S4B,E). Likewise, in sated larvae (which per se should have high Mc4r signaling), loss of Mc4r signaling increased locomotion in presence as well as in absence of food (Figures 3F and S4C,F). Analysis of swim bouts showed corresponding changes in bout frequencies and bout distances, both of which were decreased upon elevation of Mc4r signaling in fasted larvae (Figure S4B,E), but increased upon blocking Mc4r signaling in sated larvae (Figure S4C,F). These data suggest that the Mc4r system is required to mediate energy state-dependent effects on foraging- and feeding-associated locomotion in zebrafish larvae. Furthermore, under all tested conditions, Mc4r signaling has a negative effect on locomotor activity, making them swim less often (reduced bout frequency) and less far (reduced bout distance).

Modulation of locomotor activity upon acute inhibition of ARC^{Pomc} neurons in mice

To assess behavioral consequences of decreased Mc4r signaling in mice, we acutely inhibited ARC^{Pomc} neurons using a chemogenetic approach. We injected a Cre-dependent AAV containing a mutated human glycine receptor (hGlyR AAV-FLEX-hGlyR-mCherry [42] into the ARC of adult *Pomc-ires-Cre* mice (Figure 3G). Of note, the mutated hGlyR receptor responds to ivermectin (IVM) instead of its natural ligand glycine. We confirmed hGlyR expression in ARC^{Pomc} neurons as assessed by immunohistochemistry (Figure 3G). Mice expressing hGlyR in ARC^{Pomc} neurons showed significantly reduced activity in presence of food after the administration of IVM as compared to control mice (Figure 3H). IVM did not significantly change locomotor activity in absence of food (Figure S3H). We also found that hGlyR-expressing mice and control animals did not show significantly different activity levels in fasted condition, although in presence of food, activity levels were generally higher than in the absence of food (Figure S3I,J). In conclusion, ARC^{Pomc} neuron activity seems particularly required in fed mice and in the presence of food, promoting locomotor activity that is possibly involved in food intake. This is in striking contrast to the aforementioned response in zebrafish (compare Figure 3H with Figure 3F), in which under similar conditions (sated; presence of food) Mc4r signaling was required to reduce locomotor activity.

The Mc4r agonist MTII reduces the excitability of spinal zebrafish V2a neurons

We next investigated whether such opposing locomotor responses in zebrafish and mice might be associated with differences in the effects of Mc4r signaling on spinal V2a neurons. For zebrafish, Ca^{2+} imaging of V2a neuronal activity was performed in semi-intact hindbrain-spinal cord explants from transgenic larvae of 8–9 mm SL [43] with V2a-specific

GCaMP6s expression [44]. Ca^{2+} transients in V2a neurons of the precaudal spinal cord were induced by stimulating descending axons from the brainstem with an extracellular electrode that was placed at the first two spinal segments [28, 45] (Figure 4A). We confirmed that fast wash-in and wash-out of pharmacological substances was possible by bath-application of the sodium channel blocker tricaine (MESAB) or the cholinergic agonist carbachol (Figure S5E,F). Application of the Mc4r agonist MTII caused significant alterations in the amplitudes of Ca^{2+} transients in 37% (35/95) of the imaged V2a interneurons (Figure 4B–D). Of such responding neurons, 83% (29/35) displayed decreased Ca^{2+} transient amplitudes that fully reversed upon MTII washout (Figure 4D). In contrast, in the remaining 17% (6/35), Ca^{2+} transient amplitudes were increased in a non-reversible manner (Figure S5C,D). Of note, there was no apparent dorso-ventral topography of responsive versus non-responsive V2a neurons. Together, this indicates that Mc4r signaling reduces V2a interneuron excitability, in line with its inhibitory effect on locomotion as described above (Figure 3).

In most previous reports, Mc4r signaling elicits an excitatory effect on target neurons [31, 46–48], while reports of inhibitory effects are scarce [14, 49]. One such example are cholinergic neurons in the dorsal motor nucleus of the vagus (DMV) in the brainstem of adult mice. In those, Mc4r signaling induces a hyperpolarization via the activation of K_{ATP} channels, which was indicated by a reversion of the MTII effects upon co-treatment with the K_{ATP} blocker tolbutamide [14]. A similar mechanism might underlie the inhibitory effect of Mc4r signaling revealed here for V2a neurons in the zebrafish spinal cord. Thus, while tolbutamide treatment of the hindbrain-spinal cord explants per se had only minor effects (Figure S5G,H), the inhibitory effect of MTII on V2a neuronal activity was significantly reduced upon pre- and co-treatment with tolbutamide, reducing rates of MTII-responsive cells from 37% to 19% (Figure 4E,F).

Although their *mc4r* expression classifies spinal V2a neurons as potential direct targets of Pomc neurons, the described inhibition of spinal V2a neurons by Mc4r agonists could be mediated by network effects initiated by Mc4r signaling in pre-synaptic neurons. Of note, Pomca projections and *mc4r* expression were also found in the hindbrain (Figure S1D,E), known to coordinate spinal activity and locomotion [33]. To directly test whether Mc4r signaling mediates V2a neuron inhibition in absence of hindbrain input, MTII was administered to spinal preparations in which the hindbrain had been surgically separated (Figure 4G). Also in this experimental setting, the amplitudes of the electrically induced Ca^{2+} transients in precaudal V2a neurons were reduced upon MTII treatment (Figure 4H–J). Furthermore, we observed that MTII treatment reduced the amplitudes of Ca^{2+} transient in V2a neurons during fictive locomotion (Figure 4K–N). Fictive locomotion was induced by N-Methyl-D-Aspartate (NMDA) in spinal preparations that lacked the connection to the hindbrain to generate an endogenous spinal locomotor rhythm, similar as previously described [43]. Together, these studies demonstrate that Mc4r activation in fish can inhibit spinal cord V2a neurons involved in the regulation of locomotion independently of the hindbrain or other higher brain centers, suggesting direct effects.

The Mc4r agonist α-MSH excites mouse V2a neurons in spinal lamina X

To characterize the functional impact of Mc4r signaling on neurons in spinal lamina X of mice, we next performed patch clamp recordings from *Mc4r*- and *V2a*-expressing neurons (Figure 5A). Transversal thoracic spinal cord slices were prepared, and neurons were synaptically isolated (i.e., in presence of CNQX, D-AP5, picrotoxine, and strychnine) to eliminate network effects. 250 nM α-MSH was bath-applied after establishment of a stable baseline for at least 10 minutes, and the effects on membrane potential or action potential firing was measured 8–10 minutes after the onset of α-MSH administration. *Mc4r::tdTomato* neurons in lamina X were selected by their position close to the central canal (Figure 5A). The vast majority (11 out of 13) of recorded *Mc4r::tdTomato* neurons showed significant and reversible changes in action potential frequency or membrane potential (Figure 5B–D). Remarkably, α-MSH excited 7 out of 13 *Mc4r::tdTomato* neurons as indicated by an increase in action potential firing or membrane depolarization, while 4 out of 13 *Mc4r::tdTomato* neurons were inhibited (Figure 5B–D). Thus, α-MSH exerts direct and bidirectional modulatory effects on Mc4r neurons in spinal lamina X, of which two-thirds are V2a interneurons (Figure 2E).

To directly evaluate the functional impact of Mc4r signaling on spinal lamina X V2a neurons, we obtained *Chx10-Cre* mice [50], which were crossed with tdTomato reporter mice to selectively label V2a interneurons (i.e. *V2a::tdTomato*) for electrophysiological recordings (Figure 5E,F). Accurate labeling of *V2a::tdTomato* neurons in the thoracic spinal cord was confirmed by in situ hybridization (Figure 5E). Upon bath-application of α-MSH, 7 out of 12 synaptically-isolated *V2a::tdTomato* neurons were excited in a reversible manner. In the other 5 neurons, the membrane potential and action potential firing were unaffected by α-MSH (Figure 5G,H). Together, these studies demonstrate that, in mice, over half of the V2a neurons in lamina X express functional Mc4r and are positively modulated by α-MSH, in line with the positive effect of Mc4r signaling on the locomotor activity of mice as described above (Figure 3H).

Cell-type specific disruption of Mc4r signaling in zebrafish V2a neurons affects specific swimming-bout characteristics

In the zebrafish and mouse locomotor activity studies described thus far (Figure 3), Mc4r signaling was systemically blocked throughout the entire animal. To investigate the specific impact of Mc4r signaling to V2a neurons on locomotion, we generated transgenic zebrafish larvae with V2a neuron-specific expression of a dominant-negative Mc4r (dnMc4r) variant. This variant harbors a D90N exchange of the evolutionary highly conserved aspartate amino acid residue located in the second transmembrane domain of the seven transmembrane receptor (Figure 6A,B). In human, MC4R D90N heterozygosity is associated with obesity due to the loss of Mc4r signal transduction activity [5, 51]. Expression of the corresponding zebrafish dnMc4r variant driven by a V2a-specific promoter [33] resulted in moderately increased swimming velocities of sated larvae both in the absence and presence of food (Figure 6C,D). In contrast, no increases were observed in corresponding double transgenics with V2a-specific overexpression of wild-type Mc4r (data not shown). Bout analyses revealed that the increase upon expression of the dominant negative version was largely driven by a significant increase in bout frequencies (Figure 6C,D), similar to, but weaker

than the effect of systemic treatment with the Mc4r antagonist SHU9119 (Figures S4 and 6E). In contrast, average distances moved per bout, which are also increased upon SHU9119 treatment (Figure S4), were unaffected in zebrafish with V2a-specific dnMc4r expression (Figure 6C,D). Together, these data indicate that the melanocortin system does, to some extent, modulate locomotor activity via direct effects on V2a neurons, while additional targets either in the spinal cord itself (Figures 1 and 2) or in higher-order centers of the brain [33, 52] could be involved as well.

Discussion

To maintain their energy balance, animals have the options to invest energy to find food or to reduce exploratory locomotion to save energy. Previous studies have shown that the central Mc4r system, which plays a key role in maintaining energy balance, has diverse effects on locomotion. Furthermore, several brain regions harboring *Mc4r*-expressing neurons such as the PVH and the LHA have been implicated in mediating such effects of the Mc4r system on locomotion.

Here, we show that in both, zebrafish and mouse, Pomc neurons of the ARC form direct projections into locomotor control regions of the spinal cord that harbor *Mc4r*-expressing V2a interneurons as well as motoneurons. Furthermore, we not only identify V2a interneurons as previously unrecognized second-order neurons of the melanocortin system, but also show the existence of a novel, direct and evolutionary conserved mechanism of locomotor control in response to energy availability. In mouse, the Mc4r-expressing V2a interneurons, which are core elements of the CPG [23], are primarily located in lamina X [53, 54], a region clearly, and functionally, distinct from formerly reported Mc4r-expressing neurons in the IML [14, 55]. In zebrafish, these neurons are located in corresponding areas around the central canal (Figure 1 and 2). Notably, both in mouse and zebrafish, these regions also harbor other Mc4r-expressing neurons, including motoneurons, as well as V2a interneurons that lack the Mc4r. However, the latter, as well as the lack of Pomc projections into caudal-most regions of the zebrafish spinal cord, does not exclude melanocortin modulation of locomotion. Thus, V2a interneurons project caudally over several segments [56] and excitatory waves can propagate further caudal-wards in a CPG network-autonomous manner [57]. Furthermore, Pomc projections could release α-MSH also en-passant to reach even more distantly located neurons within the CPG, as formerly described for the mouse PVH [58].

Our electrophysiological and optophysiological recordings from spinal neurons of mouse and zebrafish spinal neurons confirm the functionality of the Mc4rs in both systems. The electrophysiological recordings in mice show complex and differential effects of α-MSH on different components of the spinal network. While we observed excitatory and inhibitory modulatory effects of α-MSH on Mc4r neurons that were otherwise unidentified, we found a more homogeneous and mostly excitatory effect of α-MSH on V2a neurons. Since V2a neurons tend to promote locomotion, the latter result is consistent with the reduced locomotor activity during chemogenetic inhibition of POMC neurons. Taken together, our mouse data clearly show that spinal neurons, in particular V2a neurons, are directly

modulated by α-MSH, and that modulation of the melanocortin system in vivo affects locomotor activity.

In zebrafish, more than half of the imaged V2a neurons did not respond to the applied Mc4r agonist, while the vast majority of the responding fraction displayed a diminished, rather than an increased excitability. The reasons for this limited number of responding neurons could be multifold. First, only approximately 55% of the spinal V2a neurons express *mc4r* (Figure 1L). Furthermore, according to Kimura et al. [33], most, but not all of the spinal cells labelled with the used *vsx2:gal4ff* transgene are indeed V2a neurons. We also lack definitive evidence that the effect of the Mc4r agonist on the excitability of responding V2a neurons is direct. However, it is at least to some extent independent of higher-order regulatory systems in the brain, as effects were also obtained with spinal cord explants that lacked connection to the hindbrain (Figure 4G–N). Furthermore, it is consistent with the attenuating effects of Mc4r signaling on locomotor activity of zebrafish larvae as revealed in our behavioral assays (Figures 3 and 6). Interestingly, cell type-specific transgenic blockade of Mc4r signaling in V2a neurons (Figure 6) of the hindbrain (Figure S3D,E) and spinal cord (Figures 1 and S3B’’’,C) only affected swimming bout frequencies. This is in line with the formerly described reduction in bout frequencies of free-swimming larvae in which synaptic output of V2a neurons was blocked by cell type specific expression of botulinum neurotoxin [59]. However, the average distance moved per bout, as also reduced upon systemic Mc4r inhibition throughout the entire animal, was rather unaffected upon V2a neuron-specific Mc4r inhibition. Together this suggests that direct melanocortin signaling to V2a neurons primarily affects the number of swimming events, whereas the power of individual swimming events is affected via Mc4r targets other than V2a neurons, possibly including motoneurons themselves. Neuronal activity recordings in combination with cell type-specific inhibition of Mc4r, similarly to those described here for V2a neurons, have to be performed for motoneurons to test the latter notion. Furthermore, studies involving co-labelling of recorded mouse and zebrafish V2a or Mc4r neurons, with glutamatergic, glycinergic or cholinergic markers have to reveal whether their differential responsiveness to Mc4r agonists (excitatory or inhibitory or not) is linked to differences in their neurotransmitter phenotype [60–63].

The observed differences in the behavioral responses between fish larvae and adult rodents might reflect evolutionary adaptations of an otherwise highly conserved system to their different living conditions. The main purpose of locomotion in zebrafish larvae is to search for and eventually ingest food for somatic growth. Therefore, (foraging) locomotion should be promoted when endogenous energy and Mc4r signaling levels are low but inhibited when they are high. In comparison, locomotion purposes in adult rodents are more complex, also including social activities that, in contrast to foraging, do not gain, but only cost energy. Therefore, in contrast to foraging, these types of locomotion should be promoted in times of energy surplus, likely by the associated high Mc4r signaling. Consistent with these fundamentally different purposes for locomotion and consequences with respect to energy uptake versus energy expenditure, lamina X of the mouse spinal cord harbors two different types of Mc4r target cells. Thus, we found 54% of them, including the V2a neurons, to be excited by Mc4r signaling (Figure 5), promoting locomotion in times of energy surplus, consistent with our (Figure 3G,H) and previously described behavioral tests [7, 9]. However,

31% of Mc4r target cells were inhibited by Mc4r signaling (Figure 5), possibly promoting foraging locomotion when energy depots are empty, consistent with the results obtained in other former rodent behavioral studies [10–12]. Such inhibitory effects are consistent with the responses also observed for V2a interneurons of the larval zebrafish spinal cord (Figure 4E,F), and might be mediated by similar Mc4r signaling pathways as previously described for reciprocal regulation of sympathetic and parasympathetic neurons in mammals [14]. Future cell-type-specific Mc4r knockout or reconstitution analyses need to provide ultimate proof for the functional relevance of these co-existing up- or down-regulated Mc4r target cells in the mouse spinal cord.

STAR METHODS

Resource availability

Lead contact—Further information and requests for resources and reagents should be directed to and will be fulfilled by the Lead Contact, Matthias Hammerschmidt (mhammers@uni-koeln.de).

Materials availability—Plasmids (pT2MUASzMc4r and pT2MUASdnzMc4r) generated within the course of this study are available upon request.

Data and code availability—No datasets were generated within the course of this study.

Experimental model and subject details

Experimental zebrafish models—All zebrafish care and experimental procedures were approved by the national animal care committees (LANUV Nordrhein-Westfalen; 8.87–51.05.20.10.234; 84–02.04.2012.A251; 84–02.04.2016.A390; City of Cologne; 576.1.36.6.3.01.10 Be). Zebrafish of the TL and EK strain were maintained at 27°C at a 14 h light/ 10 h dark cycle. Larvae were raised in E3 medium and fed from 5 dpf onward with paramecia culture. From 25 dpf onward, they were fed with live artemia. All larvae for behavior experiments were of both sexes in the TL background and had a SL of 8–9 mm (20–25 dpf). Preparations for anatomy were performed in animals with a SL of 9–10 mm (25–30 dpf) for technical reasons. For hindbrain-spinal cord preparations larvae with 8–9 mm SL (20–25 dpf) were used. Experimental results were not distinguished according to the gender of the animals, since gender could not be determined in larvae at the age of 20 dpf. The *Tg(pomca:EGFPras)*^{fr38Tg} line was published before [31]. *mc4r*^{sa0148} mutants [41] were obtained from the Sanger Center, Cambridge, UK. *TgBAC(vsx2:EGFP)*^{nns1Tg} [64], *Tg(vsx2:Gal4FF)*^{nns18Tg} [33] and *Tg(14xUAS:GCaMP6s)*^{mpn101Tg} [65] lines were obtained from RIKEN Center for Brain Science (Japan) and National Institute for Genetics (Japan). *Tg(mnx1:GFP)*^{ml2Tg} [66], *Tg(UAS-E1b:nfsb-mCherry)*^{c264} [67] and *nacre* −/− mutants [68] were previously described. *agrp*^{fr28} mutant zebrafish were generated during the course of this study by introducing double strand breaks using Transcription activator-like effectors (TALEN) [69]. TALEN were assembled as described earlier [70] using the Golden Gate Kit (Addgene). The forward Repeat Variable Diresidue (RVD) sequences targeting *agrp* exon 2 were NH, NH, NI, NH, HD, NI, HD, HD, NG, NG, NH, NI, NI, NI, NG and the reverse RVD's were HD, NG, NG, HD, NG, NI, NH, NG, NI, NG, HD, NG, NG,

NG, NG. Targeting constructs were cloned into the pCS2TAL3-DD und pCS2TAL3-RR vectors. TALEN constructs were in vitro transcribed after Not1 linearization using the SP6 mMessage mMachine kit (Ambion). Stable *agrp* mutant lines were generated by standard injection and screening procedures. The TALEN targeting *agrp* exon 2 caused an 8-base pair deletion at nucleotide position 179 to 186 (NM_001328012) and thereby the generation of a stop codon leading to a premature of the Agrp peptide after amino acid residue 56. Zebrafish larvae expressing dominant-negative Mc4r (dnMc4r) were generated by injecting a Nucleo Bond Xtra Midi purified plasmid (Machery-Nagel) containing Tol2 sites (pT2MUASMCS, zTrap) with inserted wild-type or D90N-modified zebrafish Mc4r together with transposase mRNA (Tol2Kit) into eggs from *vsx2:Gal4FF* transgenics. Larvae of F1 generation were used for experiments and genotyped to confirm that they contain the dnMc4r. Genomic alignments were performed using MegaX software [71].

Experimental mouse models—All mice procedures were conducted in compliance with protocols approved by local government authorities (Bezirksregierung Köln). Permission to maintain and breed mice was issued by the Department for Environment and Consumer Protection - Veterinary Section, Cologne, North Rhine-Westphalia, Germany. All animal procedures were performed in accordance with NIH guidelines. *Pomc-Cre* [72], *Pomc-ires-Cre* [73], *Mc4r-t2a-Cre* [35], *Chx10-Cre* [50], and *tdTomato* (*Ai9*) [36] mice were maintained on a mixed background and have been described previously. All Cre driver and Cre reporter mice were used in the heterozygous state. For histological studies mice between 8 and 12 weeks were used. For electrophysiological studies mice between 5 and 12 weeks were used.

Method details

Larval zebrafish feeding experiments and video recordings—We selected for larvae that were able to swim at 4 dpf. From 5 dpf on, they were transferred to plastic mouse cages filled with 200 mL of paramecia suspension. They were fed with 50 mL paramecia solution per day until they reached a standard length of 8–9 mm for behavior experiments (20–25 dpf). For low-food condition, paramecia were removed the evening before the experiment and < 500 paramecia/larva were remaining. For high-food conditions larvae were fed ad libitum with paramecia (20,000 paramecia/larva) until 30 minutes before the experiment started. For drug treatments, Melanotan II (MTII, Sigma) or SHU9119 (Tocris) were applied at 10 μM (final concentration) in system water, until 30 minutes before the recordings. Larvae were transferred in groups of 4 animals to a custom build recording arena with 102 mm diameter and 4 mm depth and dark-field illumination. A camera (Sony, HDR-CX240) was positioned above the recording chamber in a distance of 400 mm and a movie was recorded with 25 fps. Recordings were performed in a sound proof, air-conditioned room and recoding chambers were filled with fish-facility water. Locomotion was determined for 30 minutes without food and afterwards paramecia were introduced into the setup with a tubing system to record feeding behavior for additional 30 minutes. Trajectories of larvae were determined using Ctrax [74] and errors were removed by manual supervision with the fixerror script provided by the developers in Matlab (Mathworks). Velocity and total distance moved was calculated in RStudio from consecutive coordinates of the larvae as the sum per minute or sum per 30 minutes, respectively. Swim

bouts were determined using the peakfinder function in Matlab. Bouts were defined as rise in velocity over 6 mm/s. Bout duration was defined as the time between two velocity peaks. Bout speed was defined as prominence of the velocity peak. The bout distance contained the distance moved during bout + interbout.

Zebrafish in situ hybridizations—Colorimetric whole-mount in situ hybridization (WISH) of zebrafish spinal cords was carried out as described [31]. In short, 4% PFA (Sigma) fixed spinal cords were extracted from 10–11 mm SL larvae (25–30 dpf) and stored in methanol at −20°C. After rehydration they were digested with proteinase K (Genaxxon, 10 μg/mL stock, 1:1000) for 10 minutes and post-fixed with 4% PFA. Samples were blocked 2 hours in hybridization buffer (50% formamide, 2x SSC, 50 μg/μL heparin, 5 mg/mL torula-RNA (Sigma, R6625), 0.5% tween20, 5% dextransulfate, DEPC treated water). Digoxigenin (DIG, Roche) labeled probes against *mc4r* and *vsx2* (from IRBOp991H0310D) were incubated in hybridization buffer containing 10% dextransulfate (Sigma) overnight at 55 °C. Probes were washed off for total of 6 hours with SCC buffer with decreasing ionic strength. Tissue was blocked with 10% Blocking Reagent (Roche) in PBS for 2 hours following anti-DIG-AP antibody (Roche, 1:1000) in blocking solution overnight at 4 °C. The antibody was washed off for 6 hours and tissue was incubated in Nitro blue tetrazolium chloride (NBT) / 5-Brom-4-chlor-3-indoxylphosphat (BCIP) (Roche) solution in staining buffer (1:50) for 16 hours at 16°C with agitation in a 24-well plate.

Zebrafish immunohistochemistry and retrograde labeling—Zebrafish spinal cords of 10–11 mm SL (25–30 dpf) were extracted after removal of muscles and vertebral spines and 3 hours fixation with 4% PFA. They were stored in 100% methanol at −20°C over night, rehydrated and incubated in PBST (1% tritonX100, Sigma) for 3 hours at room temperature and blocked in PBST (0.5% tritonX100) with 10% fetal calf serum for 2 hours. The primary antibody against GFP (A10262, 1:500) and SV2 (AB_2315387, DSHB) was incubated in blocking solution for 2–3 days at 4°C with gentle agitation.

Retrograde labeling of axial motoneurons was performed using dye injections with tetramethylrhodamine-dextran (3000 MW; Thermo Fisher Scientific, D3308) along the pre-caudal part of the body [63].

For immunohistochemistry following colorimetric WISH for immunohistochemistry on sections, samples were cryoprotected in 30% sucrose in PBS, embedded in O.C.T cryomedium (Sakura® Finetek) and frozen at −30°C. Transverse coronal plane 20 μm thick sections were cut with a Leica cryostat. Sections were blocked with 10% FCS in PBST and incubated with primary antibody (JL-08, 1:500). Primary antibodies were detected by anti-chicken-Alexa488, anti-mouse-Alexa647 or anti-rabbit-Alexa555 (abcam).

Imaging and quantification in zebrafish—Colorimetric images of in situ hybridisations were taken with an Axio Imager M2 and using the Axiocam ICc1 (Zeiss). Fluorescent images were taken with an upright confocal microscope (LSM7, Zeiss). Merging of channels and processing of images was performed in Fiji (Image J, NIH).

Ca^{2+} imaging in zebrafish hindbrain-spinal cord explants

Explant preparation: *Tg(vsx2:Gal4FF)*^{nns18Tg} were crossed to *Tg(14xUAS:GCaMP6s)*^{mpn101Tg} fish in a nacre background [75] to reduce pigmentation. Larvae of 8–9 mm SL (20–25 dpf) were incubated in ice-cold Ringer solution (NaCl: 134 mM, KCl: 2.9 mM, $MgCl_2 \times 6H_2O$: 1.2 mM, $CaCl_2 \times 2H_2O$: 2.1 mM, HEPES: 10 mM, Glucose: 10 mM, pH = 7.8 with NaOH 10 M, 290 mOSm, bubbled with air for 3 hours at 18°C) mixed with homogenized Ringer-ice cubes and hindbrain-spinal cord explants were prepared as described [45]. The skull was removed and a cut at the level of the midbrain was performed, removing the forebrain containing the POR. Afterwards, dorsal trunk muscles and vertebral spines were removed and the hindbrain with the connected spinal cord was exposed to Ringer solution. The preparation was mounted with the dorsal side up on a Sylgard (Dow Corning) surface and was surrounded by a plastic chamber with wall degree of 30° and a volume of 1 mL. For preparations lacking the hindbrain, the preparation was cut between the hindbrain and the first 2 vertebral spines. The preparation was kept in position with 37°C warm, 1.5% low-melting point agarose (Biozym) in ringer solution. At the spinal cord from segment 1 to 12, all agarose was removed. The preparation was kept in a flow of air bubbled ringer solution at room temperature with a flow of 1 ml / minute generated by a peristaltic pump. Drugs were bath applied for 5 minutes in bubbled Ringer solution and then washed out with 10 mL Ringer solution. Melanotan II acetate (MTII, Sigma) was applied at 4–5 μM in bubbled Ringer solution, Tolbutamide (Sigma) at 2 μM and tricaine (Ethyl 3-aminobenzoate methanesulfonate, Sigma) at 0.2 mg/mL. For the pharmacologically stimulated preparation (fictive locomotion), 10 μM NMDA (Tocris) and 7 μM Tubocurarine (Sigma) was applied at and throughout the whole recording. For spinal cord explants without connectivity to the hindbrain, the preparation was performed as described above. Additionally, a cut was made between the hindbrain and the first segments of the spinal cord to rule out influence of hindbrain circuits. A 10x water-immersion objective from an Axioscop2 (Zeiss) was positioned above the first 4–8 spinal cord segments and GCaMP6s fluorescence intensity was recorded with 2 Hz and 200 ms exposure time using the Axiovision software (Zeiss).

Electrical stimulation: Spinal central pattern generators and motor circuits in the spinal cord were activated by electrical stimulation through a glass electrode made from borosilicate glass capillaries with filament (WPI) with a fire-polished tip opening of about 50–60 μm. The electrode was positioned on the dorsal surface of the CNS at the first two segments of the spinal cord as described in [43, 45] between hindbrain and spinal cord with a custom build micromanipulator fixed on the microscope stage. Every 90 seconds a stimulus with 18 repetitions of a 50 ms rectangular pulse with an amplitude of 0.6 to 1.2 mA was given for 25 minutes with a Stimulus Generator (Universal digital stimulator MS 501) connected to a Universal Stimulus Isolator (Model 401). After recording baseline activity for 5 minutes, the drug was applied for 5 minutes. After 5 minutes, the drug was washed out again. Calcium levels during washout were recorded for additional 15 minutes.

Analysis of GCaMP6s fluorescence: Ca^{2+} imaging movies were motion corrected using Stackreg plugin [76] and a region of interest was drawn around single neurons and it's mean gray value determined in Fiji (ImageJ, NIH). Data was imported into Matlab (Mathworks)

and amplitude of calcium level increases during one electrically evoked swim bout was determined using the peakfinder function. Recordings that contained calcium-level increases without electrical stimulation or movies that could not be motion corrected were excluded. V2a neurons were excluded, when the peak amplitude during baseline conditions was not stable.

Mouse surgery—Mice were anesthetized with isoflurane, received an i.p. bolus of Buprenorphin, and were placed into a stereotaxic apparatus (Kopf). Hair at the surgical site was removed and a local anesthetic agent (Lidocaine) was applied to the skin. The skull surface was exposed through a skin incision and a small drill hole was made. AAV1-FLEX-ChR2(H134R)-mCherry (Addgene, #20297) or AAV10-DIO-hGlyR-mCherry [42] were injected into the ARC of *Pomc-Cre* or *Pomc-ires-Cre*, respectively, mice (coordinates, bregma: AP: −1.45 mm, DV: −5.9 mm, ML: 0.25 mm; 200 – 300 nl) using a micromanipulator (Grass Technologies, model S48 stimulator). As control for the locomotor activity studies, AAV8-CAG-GFP (Addgene, #37825) was injected. The virus was delivered at 20–50 nl per min. For postoperative care, animals were injected intraperitoneally with Meloxicam and received tramadol in the drinking water. Mice were inspected twice daily. Body weight and health of the animals were carefully monitored until the end of the experiment. Mice with missed injections or incomplete hits were excluded from analysis after post hoc examination of mCherry expression.

Mouse brain tissue preparation for histology—Animals were terminally anesthetized and transcardially perfused with phosphate-buffered saline (PBS) followed by 10% neutral buffered formalin (PFA). Brains and spinal cord were removed, stored in the same fixative for a minimum of 2 h, transferred into 20% sucrose at 4 °C overnight. Brains were cut into 30 μm sections on a freezing microtome (Leica) coronally into four equal series. A single series of sections per animal was used in the histological studies. Spinal cords were subdivided into four segments (cervical, thoracic, lumbar and sacral) and cut into 20 μm transverse sections using a cryostat. Nine sections per animal were used for analysis.

Mouse Immunohistochemistry—Brain or spinal cord sections were washed in PBS with Tween-20, pH 7.4 (PBST) and blocked in 3% normal donkey serum in PBST for 1 h at room temperature. Sections were then incubated overnight at room temperature in blocking solution containing primary antiserum (rat anti-mCherry, Life Technologies M11217, 1:1,000; rabbit anti-Pomc precursor, Phoenix Pharmaceuticals H-029–30, 1:1,000). The next morning, sections were extensively washed in PBS and then incubated in Alexa-fluorophore secondary antibody (Molecular Probes, A-21206, A-21209, all 1:1,000) for 1 h at room temperature. After several washes in PBS, brain sections were mounted on gelatin-coated slides. Spinal cord sections were counterstained and coverslipped with DAPI containing mounting medium (VECTASHIELD® Antifade Mounting Medium with DAPI, Cat# H-1200, Vector Laboratories).

RNAscope on mouse spinal cord sections—On the day before the assay, spinal cord sections were incubated overnight at 60°C. One section from each animal was mounted to be used as negative control. Fluorescent in situ hybridization for *Vsx2*, *Chat* and *tdTomato*

mRNA detection was performed using RNA scope technique. Reagents were purchased from Advanced Cell Diagnostics (Hayward, CA), if not mentioned otherwise. In brief, sections were pre-treated for 10 min in hydrogen peroxide (Cat# 322381) at RT, followed by submersion in Target Retrieval (Cat# 322000) for 8 min at 98–99°C. The slides were rinsed twice in autoclaved Millipore water and quickly dehydrated in 100% ethanol. After air drying, a hydrophobic barrier was made around the sections using an ImmEdge hydrophobic barrier pen. The incubations were performed at 40°C, using the HybEz Hybridization System for Manual Assays. Sections were incubated for 40 min with protease IV (Cat# 322381), followed by probe hybridization for 2 h. C1-probe for *Vsx2*, no dilution, (Cat# 438341) and C3- probe for tdTomato (Cat# 317041-C3), diluted 1:50, or C2-probe for Chat (Cat# 408731-C2) and C3-probe for tdTomato, both diluted 1:50 in probe diluent (Cat# 300041) were used. A 3-plex positive (Cat# 320881) and a 3-plex negative (Cat# 320871) control probes were processed in parallel with the target probes to assess the quality of the assay. Probe hybridization was followed by 2×2 min washes in Wash buffer (Cat# 310091). The manufacturer protocol for RNAscope® Multiplex Fluorescent v2 Assay (Cat# 323110) was followed for the remaining steps (amplification and detection). Briefly, AMP1 and AMP2 were incubated for 30 min, followed by AMP3 incubation for 15 min. Between each amplification step, 2×2 min washes were performed. Afterwards a TSA Plus amplification (Perkin Elmer, Cat# NEL760001KT) protocol was used. C1- and C2-probe tyramide fluorophore was Fluorescein and C3-probe fluorophore was Cy3. DAPI was used for counterstaining and VECTASHIELD® Antifade Mounting Medium with DAPI (Cat# H-1200, Vector Laboratories) was used to coverslip the sections.

Fluorescence imaging and quantification in mouse—Images were captured using a fluorescent microscope (Keyence BZ-9000), equipped with a 20x objective (CFI Plan Apo λ20x, NA 0.75). Filter set includes a filter with excitation wavelength of 562/40 nm and an emission wavelength of 624/40 nm (Alexa A-21209, Cy3), a filter with excitation wavelength of 472.5/30 nm and an emission wavelength of 520/35 nm (Alexa A-21206, Opal520) and a filter with excitation wavelength of 377/50 nm and an emission wavelength of 447/60 nm (DAPI). Laser intensities for the different channels were kept constant throughout the imaging process. The channels were fused using ImageJ (NIH) software and images were cropped and edited with regards to brightness and contrast. Settings were applied equally across all images from both immunofluorescence and RNAscope studies. To analyze RNAscope images, positive cells in each channel within Lamina VII or X, IML, or VH of thoracic spinal cord sections were manually counted.

Mouse electrophysiology

Spinal cord slice preparation: Mice were deeply anesthetized and decapitated. A laminectomy was performed and the spinal cord was quickly removed into ice-cold cutting solution consisting of (in mM): 92 choline chloride, 30 $NaHCO_3$, 25 Glucose, 20 HEPES, 10 $MgSO_4$, 2.5 KCl, 1.25 NaH_2PO_4, 5 sodium ascorbate, 3 sodium pyruvate, 2 thiourea, 0.5 $CaCl_2$ oxygenated with 95% O_2/5% CO_2, measured osmolarity 310–320 mOsm/l. The dura mater, the dorsal and the ventral roots were removed. Transversal slices of the thoracic segment were cut at 200–300 μm thickness with a Campden vibratome (Model 7000smz-2) and incubated in oxygenated cutting solution at 34 °C for 10 min. Slices were transferred to

oxygenated aCSF consisting of (in mM; 126 NaCl, 21.4 $NaHCO_3$, 2.5 KCl, 1.2 NaH_2PO_4, 1.2 $MgCl_2$, 2.4 $CaCl_2$, 10 glucose) at 34 °C for 30 min, and stored in the same solution at room temperature (20–24 °C) for at least 60 min prior to recording.

Perforated patch clamp recordings: Perforated patch clamp experiments were performed essentially as described previously [77, 78]. Brain slices were continuously superfused with carbogenated aCSF at a flow rate of ~2.5 ml/min (recording chamber volume: ~2 ml). aCSF contained (in mM): 125 NaCl, 2.5 KCl, 2 $MgCl_2$, 2 $CaCl_2$, 1.2 NaH_2PO_4, 21 $NaHCO_3$, 10 HEPES, and 5 Glucose adjusted to pH 7.2 with NaOH. To reduce synaptic input, it contained 10^{-4} M PTX (picrotoxin, P1675, Sigma Aldrich), 50 μM DL-AP5 (DL-2-amino-5-phosphonopentanoic acid, BN0086, Biotrend), 10 μM CNQX (6-cyano-7-nitroquinoxaline-2,3-dione, C127, Sigma-Aldrich) and 5 μM strychnine (S8753, Sigma Aldrich). Current-clamp recordings of spinal *Mc4r::tdTomato* neurons *V2a::tdTomato* neurons were performed at ~32°C in the perforated patch clamp configuration. Neurons were visualized with a fixed stage upright microscope (BX51WI, Olympus, Hamburg, Germany) using 40x and 60x water-immersion objectives (LUMplan FL/N 40x, 0.8 numerical aperture, 2 mm working distance; LUMplan FL/N 60x, 1.0 numerical aperture, 2 mm working distance, Olympus) with infrared differential interference contrast optics [79] and fluorescence optics. Spinal *Mc4r::tdTomato* neurons and *V2a::tdTomato* neurons were identified according to their anatomical location and their tdTomato fluorescence. Electrodes with tip resistances between 4 and 6 MΩ were fashioned from borosilicate glass (0.86 mm inner diameter; 1.5 mm outer diameter; GB150–8P; Science Products) with a vertical pipette puller (PP-830; Narishige, London, UK).

Perforated patch experiments were conducted using protocols modified from Horn et al. [80] and Akaike et al. [81]. Recordings were performed with pipette solution containing (in mM): 140 K-gluconate, 10 KCl, 10 HEPES, 0.1 EGTA, 2 $MgCl_2$ adjusted to pH 7.2 with KOH. ATP and GTP were omitted from the intracellular solution to prevent uncontrolled permeabilization of the cell membrane [82]. The patch pipette was tip filled with internal solution and back filled with internal solution, which contained the ionophore amphotericin B (A4888; Sigma) to achieve perforated patch recordings and 0.02 % fluorescein-dextran (3000 MW, D3305, Invitrogen, Eugene, OR, USA) to monitor the stability of the perforated membrane. Amphotericin B was dissolved in dimethyl sulfoxide (DMSO; D8418, Sigma) to a concentration of 40 μg/μl following published protocols [83, 84]. The ionophore was added to the modified pipette solution shortly before use. The final concentration of amphotericin B was ~500–600 μg/ml. Amphotericin solutions were prepared from undissolved weighed samples (stored at 4°C protected from light) on the day of the recoding day. During the perforation process access resistance (R_a) was constantly monitored and experiments were started after R_a had reached steady state (~15–20 min) and the action potential amplitude was stable. To monitor the integrity of the perforated patch recording, R_a was tracked over the course of the experiment. A change to the whole-cell configuration was also indicated by fluorescein-dextran fluorescence in the cell body.

α-MSH (M4135; Sigma-Aldrich) was bath-applied (in aCSF, flow rate ~2.5 ml·min^{-1}) at a concentration of 250 nM for ~10 min. We found that the basic firing properties of spinal *Mc4r::tdTomato* neurons and *V2a::tdTomato* neurons, and their responsiveness to α-MSH

were not homogeneous. Therefore, we used the 3 σ-criterion and a neuron was considered α-MSH responsive if the change in action potential firing frequency or membrane potential induced by α-MSH was three times larger than the standard deviation. Membrane potentials and action potential frequencies were measured for 2 min under control conditions and 8–10 min after the begin of α-MSH application. For each neuron, the 2 min measuring times for control and α-MSH application were each divided into 12 bins of 10 s intervals to calculate means and respective standard deviations of action potential frequencies or membrane potentials.

Mouse locomotion assay—Starting 3–4 weeks after AAV injections, mice were singly housed, handled, and habituated to the test chamber. Mice were tested for locomotion in 30-minute trials 8 hours into the light phase (2PM). Ivermectin (IVM) was administered at a dose of 5 mg/kg via i.p. injection 24 hours prior to the assay. IVM was dissolved in a vehicle mix (60% propylene and 40% glycerol formal) at 5 mg/ml. Food was placed manually into the cage prior to the test phase. For analysis, the total distance travelled in both the x and y axis was detected using infrared light and calculated using Activity Monitor (Med Associates, Vermont USA).

Quantification and statistical analysis

Statistical analysis was performed in GraphPad Prism or InstantClue [85]. To determine differences between normally distributed experimental groups data were analyzed using the Student's two-tailed t-test or ANOVA for more than 2 groups. Differences were considered to be significant for $p < 0.05$ and significance levels are indicated in the figure legends. Data is shown as mean ± Confidence Interval for anatomy and behavior data as indicated in the figure legend. Statistics on Ca^{2+} imaging in V2a neurons was performed using the paired t-test. In graphs, columns with the same superscript letter (a,b,c) are not significantly different ($p>0.05$). Capital N shows independent replicates of the experiment, n shows the individuals of each independent N.

Supplementary Material

Refer to Web version on PubMed Central for supplementary material.

Acknowledgements

We thank the zebrafish community for sharing reagents, Dr. Kamal Sharma for sharing the mouse *Chx10-Cre* line with us, Konstantinos Ampatzis and Eva Berg for help with the zebrafish hindbrain-spinal cord explant preparations, Michael Dübbert for help with electrical stimulations, and Till Bockemühl for help with the swim bout analyses. Work in MH's laboratory was supported by the Deutsche Forschungsgemeinschaft (DFG, German Research Foundation) – 233886668 / GRK 1960, and the US National Institute of General Medical Sciences (GM63904). Work in HF's laboratory was supported by the DFG grant 409551513.

References

1. Waterson MJ, and Horvath TL (2015). Neuronal Regulation of Energy Homeostasis: Beyond the Hypothalamus and Feeding. Cell metabolism 22, 962–970. [PubMed: 26603190]
2. Timper K, and Brüning JC (2017). Hypothalamic circuits regulating appetite and energy homeostasis: pathways to obesity. Dis Model Mech 10, 679–689. [PubMed: 28592656]

3. Souza FSJ, Bumaschny VF, Low MJ, and Rubinstein M (2005). Subfunctionalization of expression and peptide domains following the ancient duplication of the proopiomelanocortin gene in teleost fishes. Mol Biol Evol 22, 2417–2427. [PubMed: 16093565]
4. Huszar D, Lynch CA, Fairchild-Huntress V, Dunmore JH, Fang Q, Berkemeier LR, Gu W, Kesterson RA, Boston BA, Cone RD, et al. (1997). Targeted disruption of the melanocortin-4 receptor results in obesity in mice. Cell 88, 131–141. [PubMed: 9019399]
5. Biebermann H, Krude H, Elsner A, Chubanov V, Gudermann T, and Gruters A (2003). Autosomal-dominant mode of inheritance of a melanocortin-4 receptor mutation in a patient with severe early-onset obesity is due to a dominant-negative effect caused by receptor dimerization. Diabetes 52, 2984–2988. [PubMed: 14633860]
6. Schiöth HB, Haitina T, Ling MK, Ringholm A, Fredriksson R, Cerdá-Reverter JM, and Klovins J (2005). Evolutionary conservation of the structural, pharmacological, and genomic characteristics of the melanocortin receptor subtypes. Peptides 26, 1886–1900. [PubMed: 15985310]
7. Lute B, Jou W, Lateef DM, Goldgof M, Xiao C, Pinol RA, Kravitz AV, Miller NR, Huang YG, Girardet C, et al. (2014). Biphasic effect of melanocortin agonists on metabolic rate and body temperature. Cell Metab 20, 333–345. [PubMed: 24981835]
8. Adage T, Scheurink AJ, de Boer SF, de Vries K, Konsman JP, Kuipers F, Adan RA, Baskin DG, Schwartz MW, and van Dijk G (2001). Hypothalamic, metabolic, and behavioral responses to pharmacological inhibition of CNS melanocortin signaling in rats. J Neurosci 21, 3639–3645. [PubMed: 11331393]
9. Ste Marie L, Miura GI, Marsh DJ, Yagaloff K, and Palmiter RD (2000). A metabolic defect promotes obesity in mice lacking melanocortin-4 receptors. Proc Natl Acad Sci U S A 97, 12339–12344. [PubMed: 11027312]
10. Krashes MJ, Koda S, Ye C, Rogan SC, Adams AC, Cusher DS, Maratos-Flier E, Roth BL, and Lowell BB (2011). Rapid, reversible activation of AgRP neurons drives feeding behavior in mice. J Clin Invest 121, 1424–1428. [PubMed: 21364278]
11. Dietrich MO, Zimmer MR, Bober J, and Horvath TL (2015). Hypothalamic Agrp neurons drive stereotypic behaviors beyond feeding. Cell 160, 1222–1232. [PubMed: 25748653]
12. Schuhler S, Horan TL, Hastings MH, Mercer JG, Morgan PJ, and Ebling FJ (2004). Feeding and behavioural effects of central administration of the melanocortin 3/4-R antagonist SHU9119 in obese and lean Siberian hamsters. Behav Brain Res 152, 177–185.
13. Elias CF, Lee C, Kelly J, Aschkenasi C, Ahima RS, Couceyro PR, Kuhar MJ, Saper CB, and Elmquist JK (1998). Leptin activates hypothalamic CART neurons projecting to the spinal cord. Neuron 21, 1375–1385. [PubMed: 9883730]
14. Sohn J-W, Harris LE, Berglund ED, Liu T, Vong L, Lowell BB, Balthasar N, Williams KW, and Elmquist JK (2013). Melanocortin 4 receptors reciprocally regulate sympathetic and parasympathetic preganglionic neurons. Cell 152, 612–619. [PubMed: 23374353]
15. Skibicka KP, and Grill HJ (2009). Hypothalamic and hindbrain melanocortin receptors contribute to the feeding, thermogenic, and cardiovascular action of melanocortins. Endocrinology 150, 5351–5361. [PubMed: 19854868]
16. Pei H, Patterson CM, Sutton AK, Burnett KH, Myers MG Jr., and Olson DP (2019). Lateral Hypothalamic Mc3R-Expressing Neurons Modulate Locomotor Activity, Energy Expenditure, and Adiposity in Male Mice. Endocrinology 160, 343–358. [PubMed: 30541071]
17. Hill JW, and Faulkner LD (2017). The Role of the Melanocortin System in Metabolic Disease: New Developments and Advances. Neuroendocrinology 104, 330–346. [PubMed: 27728914]
18. Wyart C (2018). Taking a Big Step towards Understanding Locomotion. Trends Neurosci 41, 869–870. [PubMed: 30471663]
19. Berg EM, Björnfors ER, Pallucchi I, Picton LD, and El Manira A (2018). Principles Governing Locomotion in Vertebrates. Front Neural Circuits 12, 223.
20. Kiehn O (2016). Decoding the organization of spinal circuits that control locomotion. Nat Rev Neurosci 17, 224–238. [PubMed: 26935168]
21. Fetcho JR, and McLean DL (2010). Some principles of organization of spinal neurons underlying locomotion in zebrafish and their implications. Ann N Y Acad Sci 1198, 94–104. [PubMed: 20536924]

22. Crone SA, Quinlan KA, Zagoraiou L, Droho S, Restrepo CE, Lundfald L, Endo T, Setlak J, Jessell TM, Kiehn O, et al. (2008). Genetic ablation of V2a ipsilateral interneurons disrupts left-right locomotor coordination in mammalian spinal cord. Neuron 60, 70–83. [PubMed: 18940589]
23. Dougherty KJ, and Kiehn O (2010). Firing and cellular properties of V2a interneurons in the rodent spinal cord. J. Neurosci. 30, 24–37. [PubMed: 20053884]
24. McLean DL, Fan J, Higashijima S, Hale ME, and Fetcho JR (2007). A topographic map of recruitment in spinal cord. Nature 446, 71–75. [PubMed: 17330042]
25. McLean DL, Masino MA, Koh IY, Lindquist WB, and Fetcho JR (2008). Continuous shifts in the active set of spinal interneurons during changes in locomotor speed. Nat Neurosci 11, 1419–1429. [PubMed: 18997790]
26. McLean DL, and Fetcho JR (2009). Spinal interneurons differentiate sequentially from those driving the fastest swimming movements in larval zebrafish to those driving the slowest ones. J Neurosci 29, 13566–13577. [PubMed: 19864569]
27. Menelaou E, and McLean DL (2013). Speed control: spinal interneurons with crossed purposes. Curr Biol 23, R716–718. [PubMed: 24028949]
28. Ampatzis K, Song J, Ausborn J, and El Manira A (2014). Separate microcircuit modules of distinct v2a interneurons and motoneurons control the speed of locomotion. Neuron 83, 934–943. [PubMed: 25123308]
29. Song J, Ampatzis K, Björnfors ER, and El Manira A (2016). Motor neurons control locomotor circuit function retrogradely via gap junctions. Nature 529, 399–402. [PubMed: 26760208]
30. Eklof-Ljunggren E, Haupt S, Ausborn J, Dehnisch I, Uhlen P, Higashijima S, and El Manira A (2012). Origin of excitation underlying locomotion in the spinal circuit of zebrafish. Proc Natl Acad Sci U S A 109, 5511–5516. [PubMed: 22431619]
31. Löhr H, Hess S, Pereira MMA, Reinoss P, Leibold S, Schenkel C, Wunderlich CM, Kloppenburg P, Bruning JC, and Hammerschmidt M (2018). Diet-Induced Growth Is Regulated via Acquired Leptin Resistance and Engages a Pomc-Somatostatin-Growth Hormone Circuit. Cell Rep 23, 1728–1741. [PubMed: 29742429]
32. Stil A, and Drapeau P (2016). Neuronal labeling patterns in the spinal cord of adult transgenic Zebrafish. Dev Neurobiol 76, 642–660. [PubMed: 26408263]
33. Kimura Y, Satou C, Fujioka S, Shoji W, Umeda K, Ishizuka T, Yawo H, and Higashijima S (2013). Hindbrain V2a neurons in the excitation of spinal locomotor circuits during zebrafish swimming. Curr Biol 23, 843–849. [PubMed: 23623549]
34. Krashes MJ, Lowell BB, and Garfield AS (2016). Melanocortin-4 receptor-regulated energy homeostasis. Nat Neurosci 19, 206–219. [PubMed: 26814590]
35. Garfield AS, Li C, Madara JC, Shah BP, Webber E, Steger JS, Campbell JN, Gavrilova O, Lee CE, Olson DP, et al. (2015). A neural basis for melanocortin-4 receptor-regulated appetite. Nat Neurosci 18, 863–871. [PubMed: 25915476]
36. Madisen L, Zwingman TA, Sunkin SM, Oh SW, Zariwala HA, Gu H, Ng LL, Palmiter RD, Hawrylycz MJ, Jones AR, et al. (2010). A robust and high-throughput Cre reporting and characterization system for the whole mouse brain. Nat Neurosci 13, 133–140. [PubMed: 20023653]
37. Horstick EJ, Bayleyen Y, Sinclair JL, and Burgess HA (2017). Search strategy is regulated by somatostatin signaling and deep brain photoreceptors in zebrafish. BMC Biol 15, 4. [PubMed: 28122559]
38. Johnson RE, Linderman S, Panier T, Wee CL, Song E, Herrera KJ, Miller A, and Engert F (2020). Probabilistic Models of Larval Zebrafish Behavior Reveal Structure on Many Scales. Curr Biol 30, 70–82.e74. [PubMed: 31866367]
39. Anderson EJP, Cakir I, Carrington SJ, Cone RD, Ghamari-Langroudi M, Gillyard T, Gimenez LE, and Litt MJ (2016). 60 YEARS OF POMC: Regulation of feeding and energy homeostasis by alpha-MSH. J Mol Endocrinol 56, T157–174. [PubMed: 26939593]
40. Sutton GM, Josephine Babin M, Gu X, Hruby VJ, and Butler AA (2008). A derivative of the melanocortin receptor antagonist SHU9119 (PG932) increases food intake when administered peripherally. Peptides 29, 104–111. [PubMed: 18054119]

41. Zhang C, Forlano PM, and Cone RD (2012). AgRP and POMC neurons are hypophysiotropic and coordinately regulate multiple endocrine axes in a larval teleost. Cell Metab 15, 256–264. [PubMed: 22245570]
42. Todd WD, Fenselau H, Wang JL, Zhang R, Machado NL, Venner A, Broadhurst RY, Kaur S, Lynagh T, Olson DP, et al. (2018). A hypothalamic circuit for the circadian control of aggression. Nat Neurosci 21, 717–724. [PubMed: 29632359]
43. Kyriakatos A, Mahmood R, Ausborn J, Porres CP, Buschges A, and El Manira A (2011). Initiation of locomotion in adult zebrafish. J Neurosci 31, 8422–8431. [PubMed: 21653846]
44. Muto A, Ohkura M, Kotani T, Higashijima S. i., Nakai J, and Kawakami K (2011). Genetic visualization with an improved GCaMP calcium indicator reveals spatiotemporal activation of the spinal motor neurons in zebrafish. Proc Natl Acad Sci U S A 108, 5425–5430. [PubMed: 21383146]
45. Ampatzis K, Song J, Ausborn J, and El Manira A (2013). Pattern of innervation and recruitment of different classes of motoneurons in adult zebrafish. J Neurosci 33, 10875–10886. [PubMed: 23804107]
46. Smith MA, Hisadome K, Al-Qassab H, Heffron H, Withers DJ, and Ashford ML (2007). Melanocortins and agouti-related protein modulate the excitability of two arcuate nucleus neuron populations by alteration of resting potassium conductances. J Physiol 578, 425–438. [PubMed: 17068101]
47. Wan S, Browning KN, Coleman FH, Sutton G, Zheng H, Butler A, Berthoud HR, and Travagli RA (2008). Presynaptic melanocortin-4 receptors on vagal afferent fibers modulate the excitability of rat nucleus tractus solitarius neurons. J Neurosci 28, 4957–4966. [PubMed: 18463249]
48. Ghamari-Langroudi M, Digby GJ, Sebag JA, Millhauser GL, Palomino R, Matthews R, Gillyard T, Panaro BL, Tough IR, Cox HM, et al. (2015). G-protein-independent coupling of MC4R to Kir7.1 in hypothalamic neurons. Nature 520, 94–98. [PubMed: 25600267]
49. Fu LY, and van den Pol AN (2008). Agouti-related peptide and MC3/4 receptor agonists both inhibit excitatory hypothalamic ventromedial nucleus neurons. J Neurosci 28, 5433–5449. [PubMed: 18495877]
50. Azim E, Jiang J, Alstermark B, and Jessell TM (2014). Skilled reaching relies on a V2a propriospinal internal copy circuit. Nature 508, 357–363. [PubMed: 24487617]
51. Lotta LA, Mokrosiński J, Mendes de Oliveira E, Li C, Sharp SJ, Luan J, Brouwers B, Ayinampudi V, Bowker N, Kerrison N, et al. (2019). Human Gain-of-Function MC4R Variants Show Signaling Bias and Protect against Obesity. Cell 177, 597–607.e599. [PubMed: 31002796]
52. Wee CL, Song EY, Johnson RE, Ailani D, Randlett O, Kim JY, Nikitchenko M, Bahl A, Yang CT, Ahrens MB, et al. (2019). A bidirectional network for appetite control in larval zebrafish. Elife 8, e43775. [PubMed: 31625906]
53. Stepien AE, Tripodi M, and Arber S (2010). Monosynaptic rabies virus reveals premotor network organization and synaptic specificity of cholinergic partition cells. Neuron 68, 456–472. [PubMed: 21040847]
54. Kiehn O, and Kjaerulff O (1998). Distribution of central pattern generators for rhythmic motor outputs in the spinal cord of limbed vertebrates. Ann N Y Acad Sci 860, 110–129. [PubMed: 9928306]
55. Gautron L, Lee CE, Lee S, and Elmquist JK (2012). Melanocortin-4 receptor expression in different classes of spinal and vagal primary afferent neurons in the mouse. J Comp Neurol 520, 3933–3948. [PubMed: 22592759]
56. Menelaou E, VanDunk C, and McLean DL (2014). Differences in the morphology of spinal V2a neurons reflect their recruitment order during swimming in larval zebrafish. J Comp Neurol 522, 1232–1248. [PubMed: 24114934]
57. Fidelin K, Djenoune L, Stokes C, Prendergast A, Gomez J, Baradel A, Del Bene F, and Wyart C (2015). State-Dependent Modulation of Locomotion by GABAergic Spinal Sensory Neurons. Curr Biol 25, 3035–3047. [PubMed: 26752076]
58. Atasoy D, Betley JN, Li W-P, Su HH, Sertel SM, Scheffer LK, Simpson JH, Fetter RD, and Sternson SM (2014). A genetically specified connectomics approach applied to long-range feeding regulatory circuits. Nat Neurosci 17, 1830–1839. [PubMed: 25362474]

59. Sternberg JR, Severi KE, Fidelin K, Gomez J, Ihara H, Alcheikh Y, Hubbard JM, Kawakami K, Suster M, and Wyart C (2016). Optimization of a Neurotoxin to Investigate the Contribution of Excitatory Interneurons to Speed Modulation In Vivo. Curr Biol 26, 2319–2328. [PubMed: 27524486]
60. Lundfald L, Restrepo CE, Butt SJ, Peng CY, Droho S, Endo T, Zeilhofer HU, Sharma K, and Kiehn O (2007). Phenotype of V2-derived interneurons and their relationship to the axon guidance molecule EphA4 in the developing mouse spinal cord. Eur J Neurosci 26, 2989–3002. [PubMed: 18028107]
61. Delile J, Rayon T, Melchionda M, Edwards A, Briscoe J, and Sagner A (2019). Single cell transcriptomics reveals spatial and temporal dynamics of gene expression in the developing mouse spinal cord. Development 146.
62. Menelaou E, and McLean DL (2019). Hierarchical control of locomotion by distinct types of spinal V2a interneurons in zebrafish. Nat Commun 10, 4197. [PubMed: 31519892]
63. Pedroni A, and Ampatzis K (2019). Large-Scale Analysis of the Diversity and Complexity of the Adult Spinal Cord Neurotransmitter Typology. iScience 19, 1189–1201. [PubMed: 31542702]
64. Kimura Y, Okamura Y, and Higashijima S (2006). alx, a zebrafish homolog of Chx10, marks ipsilateral descending excitatory interneurons that participate in the regulation of spinal locomotor circuits. J Neurosci 26, 5684–5697. [PubMed: 16723525]
65. Thiele TR, Donovan JC, and Baier H (2014). Descending control of swim posture by a midbrain nucleus in zebrafish. Neuron 83, 679–691. [PubMed: 25066082]
66. Flanagan-Steet H, Fox MA, Meyer D, and Sanes JR (2005). Neuromuscular synapses can form in vivo by incorporation of initially aneural postsynaptic specializations. Development 132, 4471–4481. [PubMed: 16162647]
67. Davison JM, Akitake CM, Goll MG, Rhee JM, Gosse N, Baier H, Halpern ME, Leach SD, and Parsons MJ (2007). Transactivation from Gal4-VP16 transgenic insertions for tissue-specific cell labeling and ablation in zebrafish. Dev Biol 304, 811–824. [PubMed: 17335798]
68. Lister JA, Robertson CP, Lepage T, Johnson SL, and Raible DW (1999). nacre encodes a zebrafish microphthalmia-related protein that regulates neural-crest-derived pigment cell fate. Development 126, 3757–3767. [PubMed: 10433906]
69. Ma AC, Chen Y, Blackburn PR, and Ekker SC (2016). TALEN-Mediated Mutagenesis and Genome Editing. Methods Mol Biol 1451, 17–30. [PubMed: 27464798]
70. Cermak T, Doyle EL, Christian M, Wang L, Zhang Y, Schmidt C, Baller JA, Somia NV, Bogdanove AJ, and Voytas DF (2011). Efficient design and assembly of custom TALEN and other TAL effector-based constructs for DNA targeting. Nucleic Acids Res 39, e82. [PubMed: 21493687]
71. Kumar S, Stecher G, Li M, Knyaz C, and Tamura K (2018). MEGA X: Molecular Evolutionary Genetics Analysis across Computing Platforms. Mol Biol Evol 35, 1547–1549. [PubMed: 29722887]
72. Balthasar N, Coppari R, McMinn J, Liu SM, Lee CE, Tang V, Kenny CD, McGovern RA, Chua SC Jr., Elmquist JK, et al. (2004). Leptin receptor signaling in POMC neurons is required for normal body weight homeostasis. Neuron 42, 983–991. [PubMed: 15207242]
73. Fenselau H, Campbell JN, Verstegen AM, Madara JC, Xu J, Shah BP, Resch JM, Yang Z, Mandelblat-Cerf Y, Livneh Y, et al. (2017). A rapidly acting glutamatergic ARC→PVH satiety circuit postsynaptically regulated by α-MSH. Nat Neurosc 20, 42–51.
74. Branson K, Robie AA, Bender J, Perona P, and Dickinson MH (2009). High-throughput ethomics in large groups of Drosophila. Nat Methods 6, 451–457. [PubMed: 19412169]
75. White RM, Sessa A, Burke C, Bowman T, LeBlanc J, Ceol C, Bourque C, Dovey M, Goessling W, Burns CE, et al. (2008). Transparent adult zebrafish as a tool for in vivo transplantation analysis. Cell Stem Cell 2, 183–189. [PubMed: 18371439]
76. Thévenaz P, Ruttimann UE, and Unser M (1998). A pyramid approach to subpixel registration based on intensity. IEEE Trans Image Process 7, 27–41. [PubMed: 18267377]
77. Hess ME, Hess S, Meyer KD, Verhagen LA, Koch L, Bronneke HS, Dietrich MO, Jordan SD, Saletore Y, Elemento O, et al. (2013). The fat mass and obesity associated gene (Fto)

regulates activity of the dopaminergic midbrain circuitry. Nat Neurosci 16, 1042–1048. [PubMed: 23817550]

78. Konner AC, Hess S, Tovar S, Mesaros A, Sanchez-Lasheras C, Evers N, Verhagen LA, Bronneke HS, Kleinridders A, Hampel B, et al. (2011). Role for insulin signaling in catecholaminergic neurons in control of energy homeostasis. Cell Metab 13, 720–728. [PubMed: 21641553]
79. Dodt HU, and Zieglgansberger W (1990). Visualizing unstained neurons in living brain slices by infrared DIC-videomicroscopy. Brain Res 537, 333–336. [PubMed: 2085783]
80. Horn R, and Marty A (1988). Muscarinic activation of ionic currents measured by a new whole-cell recording method. J Gen Physiol 92, 145–159. [PubMed: 2459299]
81. Akaike N, and Harata N (1994). Nystatin perforated patch recording and its applications to analyses of intracellular mechanisms. Jpn J Physiol 44, 433–473. [PubMed: 7534361]
82. Lindau M, and Fernandez JM (1986). IgE-mediated degranulation of mast cells does not require opening of ion channels. Nature 319, 150–153. [PubMed: 2417125]
83. Rae J, Cooper K, Gates P, and Watsky M (1991). Low access resistance perforated patch recordings using amphotericin B. J Neurosci Methods 37, 15–26. [PubMed: 2072734]
84. Kyrozis A, and Reichling DB (1995). Perforated-patch recording with gramicidin avoids artifactual changes in intracellular chloride concentration. J Neurosci Methods 57, 27–35. [PubMed: 7540702]
85. Nolte H, MacVicar TD, Tellkamp F, and Krüger M (2018). Instant Clue. Sci Rep 8, 12648. [PubMed: 30140043]

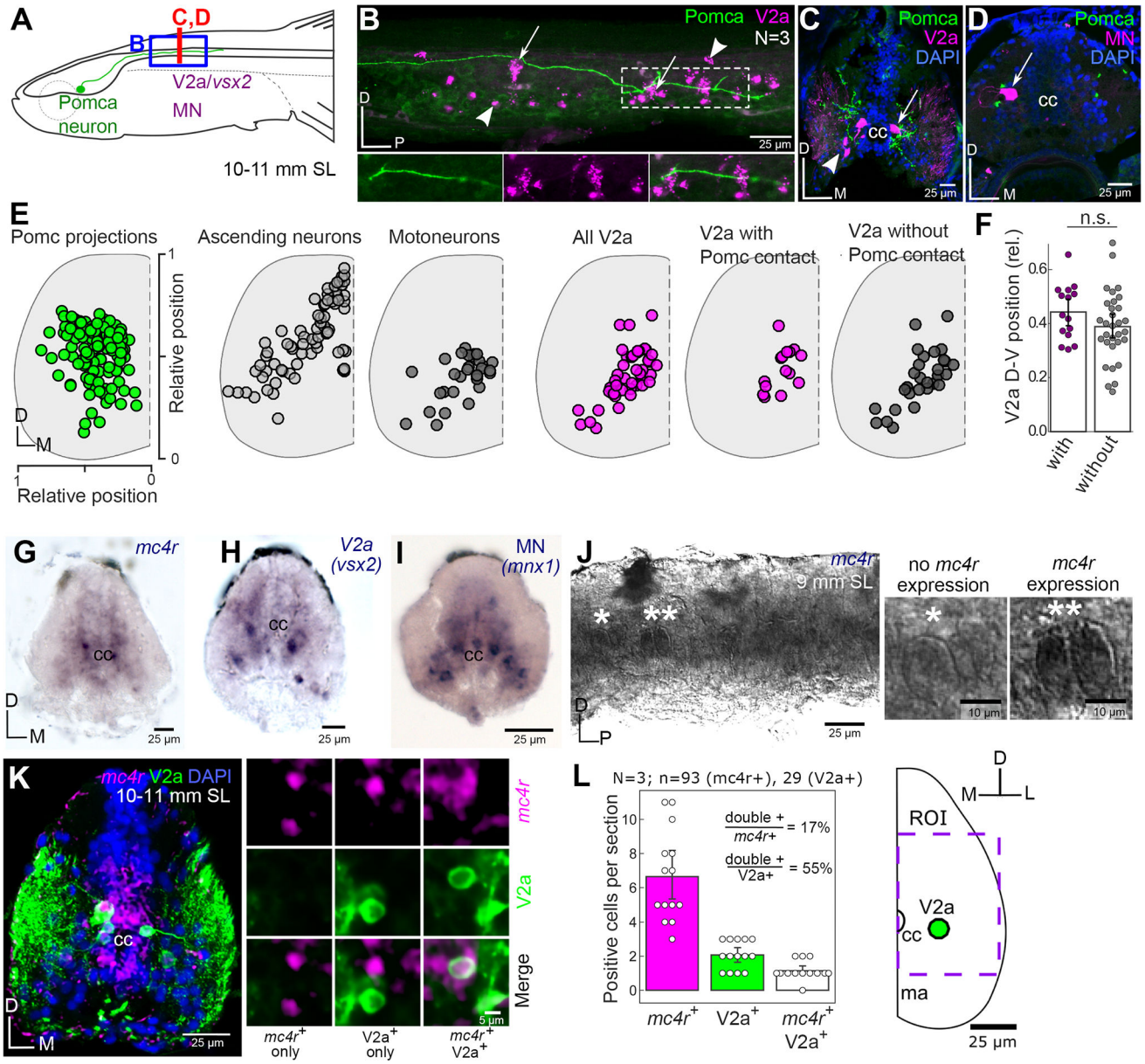

Figure 1: Pomca neurons target spinal (pre-)motor circuits in zebrafish larvae

(A) Schematic illustration of the imaged region. (B-D) Immunohistochemistry of *pomca:EGFPras* crossed to *vsx2:Gal4FF; UAS-E1b:nfsb-mCherry* transgenic larvae of 10–11 mm standard length (SL). B shows lateral view of whole mount spinal cord preparation; upper panel shows maximum intensity projection; for boxed region, single plane images are shown below (see also Supplemental Video 1 for Z-stack). C and D show transverse sections of the spinal cord. (C) Pomca projections are in proximity (arrow) or more distant (arrowhead) to V2a neurons. (D) Motoneurons backfilled with rhodamine-dextran in proximity to Pomca projections. (E) Dorso-ventral topology of Pomca projections in transverse sections of the spinal cord at SL 10. Position of ascending neurons adapted from Pedroni and Ampatzis [63]. (F) Dorso-ventral quantification of Pomca and V2a contacts. (G-I) Colorimetric in situ hybridization for *mc4r*, *vsx2* and *gfp* (in *mnx1:GFP* transgenic

animal) on spinal transverse sections at 9–10 mm SL. (J) Lateral view of whole mount spinal cord at 9 mm SL stained with colorimetric in-situ hybridization against *mc4r*. Motoneurons without signal (arrowhead) and with signal (arrow) are magnified in the right panel. (K) *mc4r* colorimetric in situ hybridization signal overlapped with fluorescence of V2a neurons of *vsx2:GFP* transgenic animal. Right panels show magnified views of exemplary neurons of indicated categories from different sections. (L) Quantification of co-localization in images as in (K) and the defined regions of interest (ROI, right panel). N = 3 animals, n = 9 spinal cord sections. cc, central canal; D, dorsal; P, posterior; M, medial; L, lateral; n.s., not significant. See also Figure S1.

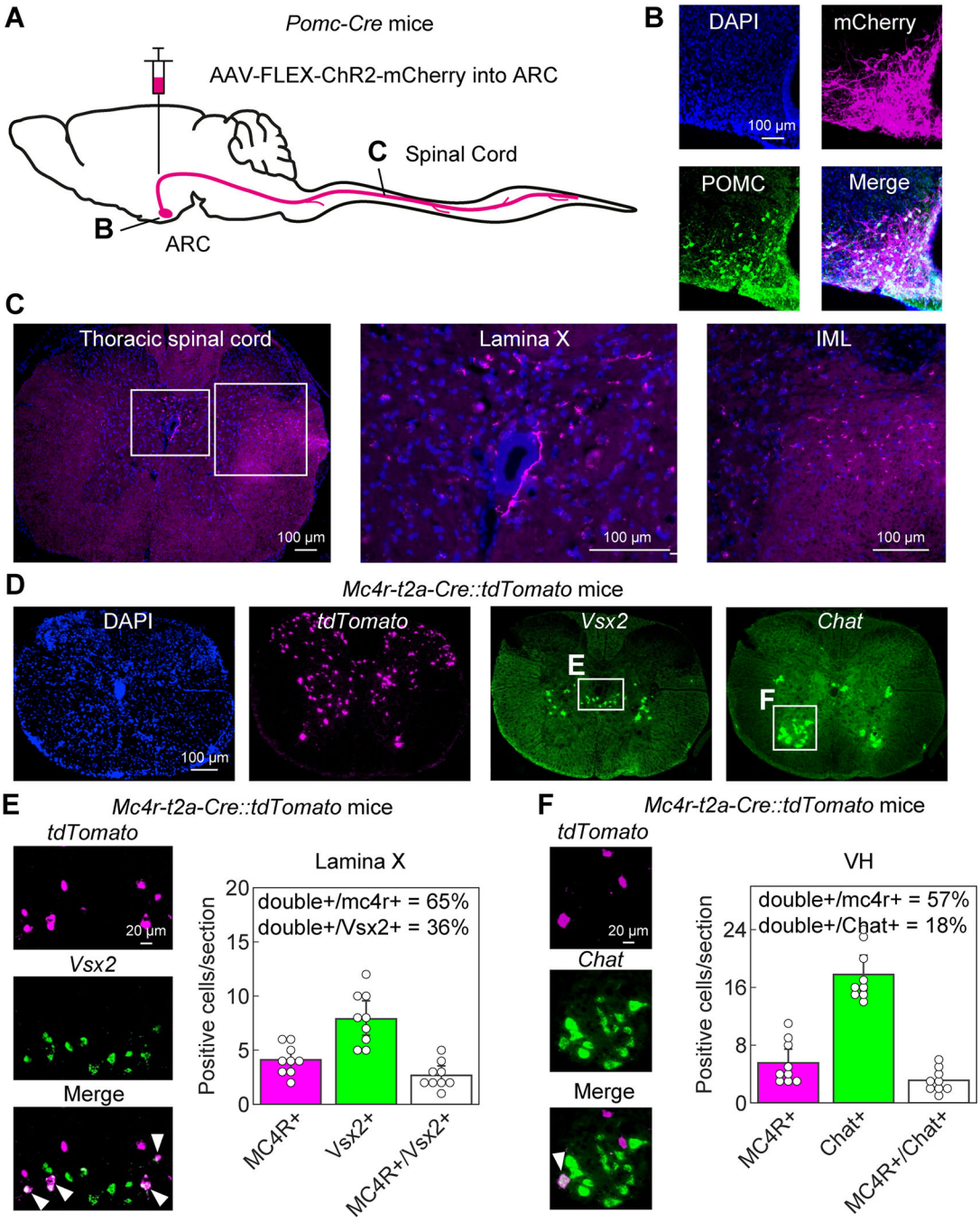

Figure 2: Mouse ARC^{Pomc} neurons send long-range projection to spinal lamina X, where *Vsx2* marks *Mc4r*-expressing neurons

(A) Schematic illustrating Cre-dependent labelling of ARC^{Pomc} neuron axonal terminals with ChR2-mCherry. (B) Colocalization of Pomc protein in ChR2-mCherry-positive ARC^{Pomc} neurons. (C) ChR2-mCherry immunolabeling of ARC^{Pomc} neuron projections in the thoracic spinal cord in lamina X and in the IML. (D-F) Colocalization of *Vsx2* and *Chat* RNA in *Mc4r::tdTomato* neurons in lamina X and in the VH of the thoracic spinal cord. (E, F) Summary of *Mc4r::tdTomato* neurons in spinal lamina X that express *Vsx2* RNA

(E) and in VH neurons that express *Chat*. ARC, arcuate nucleus of the hypothalamus; IML, intermediolateral cell column. See also Figure S2.

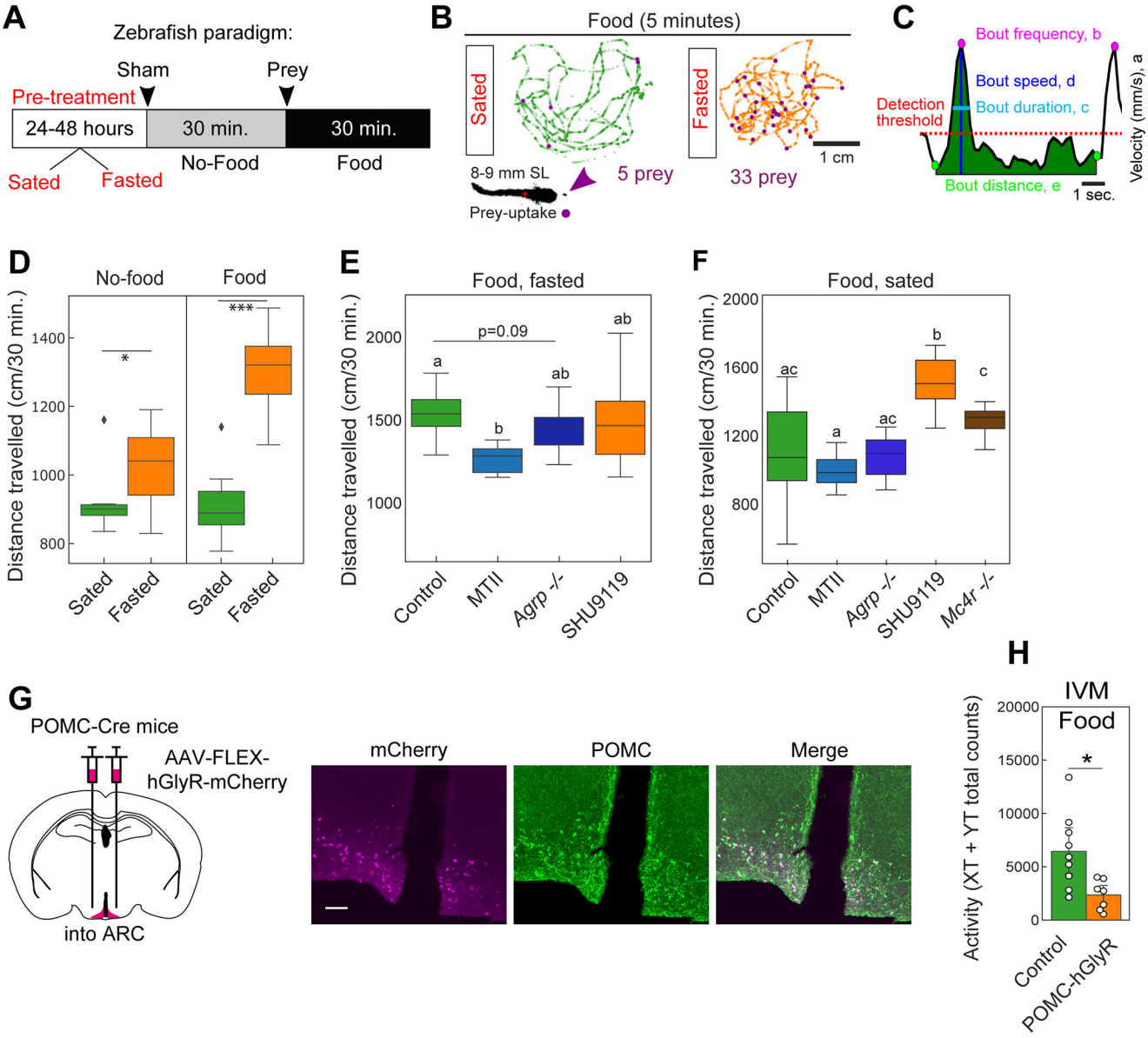

Figure 3. Manipulation of the Mc4r system affects locomotor activity in zebrafish and mice

(A) Behavior paradigm for video recordings of fasted or sated larvae at 8–9 mm SL. (B) Representative trajectories of 5 minutes high magnification video recordings of a fasted and sated larva in the presence of paramecia (prey), with individual paramecia uptake events indicated by purple circles. (C) Plot shows velocity over time and the threshold (dashed line, 6 mm/s) to detect a swim-bout. (D) Plots depicting increased locomotion of fasted compared to sated larvae during foraging and feeding (N = 12). (E) Distance travelled in presence of food in fasted and sated (F) larvae (* = $p<0.05$, ** = $p<0.01$, N = 12). (G) Experimental schematic in mice (left) and expression of Cre-dependent AAV-FLEX-hGlyR-mCherry in ARC^{Pomc} neurons (right) as determined by immunolabeling. (H) effects of hGlyR/Ivermectin-induced inhibition of mouse ARC^{Pomc} neurons on locomotor activity in presence of food. See also Figures S3–S4.

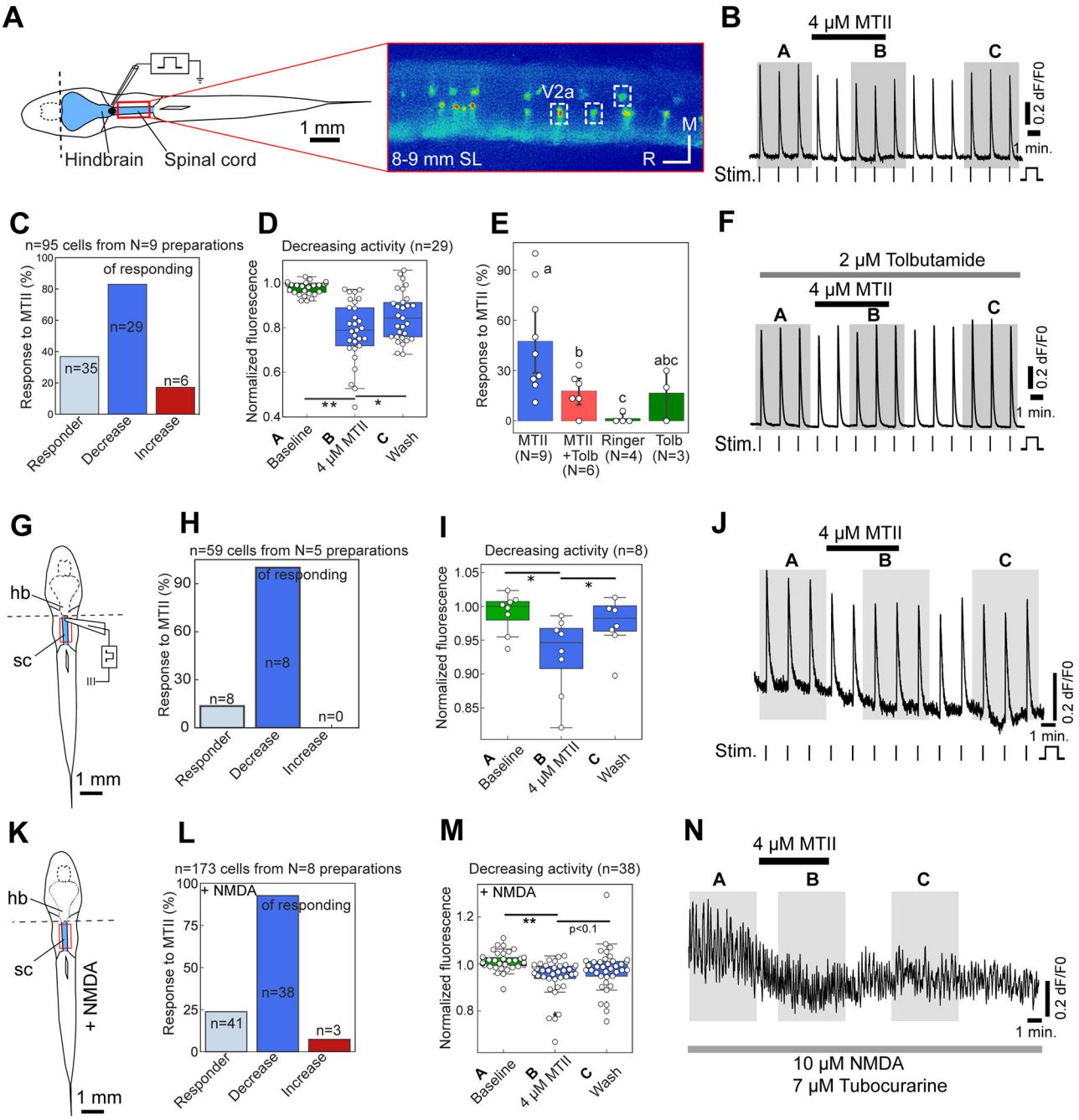

Figure 4: Zebrafish spinal networks respond to the Mc4r agonist MTII

(A) Schematic illustration of the hindbrain-spinal cord preparation (in blue) and exemplary still of Ca^{2+} transients in spinal V2a neurons of *vsx2:Gal4FF*; *14xUAS:GCaMP6s* larvae of 8–9 mm SL fasted for one day, with settings allowing simultaneous recordings in all dorso-ventral planes of the spinal cord. (B) Exemplary recording of individual V2a interneuron showing decreased Ca^{2+} transients upon bath application of 4–5 µM MTII. Horizontal bars indicate when MTII, vertical bars when the electrical stimuli (Stim) were applied. Shaded areas (A,B,C) indicate when Ca^{2+} transients were quantified for panels (D,I,M). (C) Percentages of V2a neurons responding to applied MTII according to 3-σ criterion

(see STAR methods). (D) Percentages of V2a neurons in which evoked Ca^{2+} transients were reduced by MTII in a reversible manner. (E,F) The K-ATPase blocker tolbutamide (Tolb, 2 μM) had no major effect on Ca^{2+} transients ($p = 0.81$), but prevented the normally decreasing effect of MTII ($p = 0.01$). (G-J) Schematic illustration of hindbrain-spinal cord preparation for electrical stimulation with section (dashed line) between hindbrain and spinal cord (G), percentages of V2a neurons responding to applied MTII (H), fluorescence values for V2a neurons with a reversible negative response (I), and exemplary recording of individual electrically stimulated V2a interneuron (J). (K-N) Schematic illustration of hindbrain-spinal cord preparation for 10 μM NMDA stimulation with section between hindbrain and spinal cord (K), percentages of V2a neurons responding to applied MTII (L) fluorescence values for V2a neurons with a reversible negative response (M), and exemplary recording of individual NMDA-stimulated V2a interneuron. Tubocurarine was used to prevent muscle contractions. Columns show mean ± confidence intervals; columns with the same superscript letter (a,b,c) are not significantly different ($p>0.05$); * = $p<0.05$, ** = $p<0.01$. See also Figure S5.

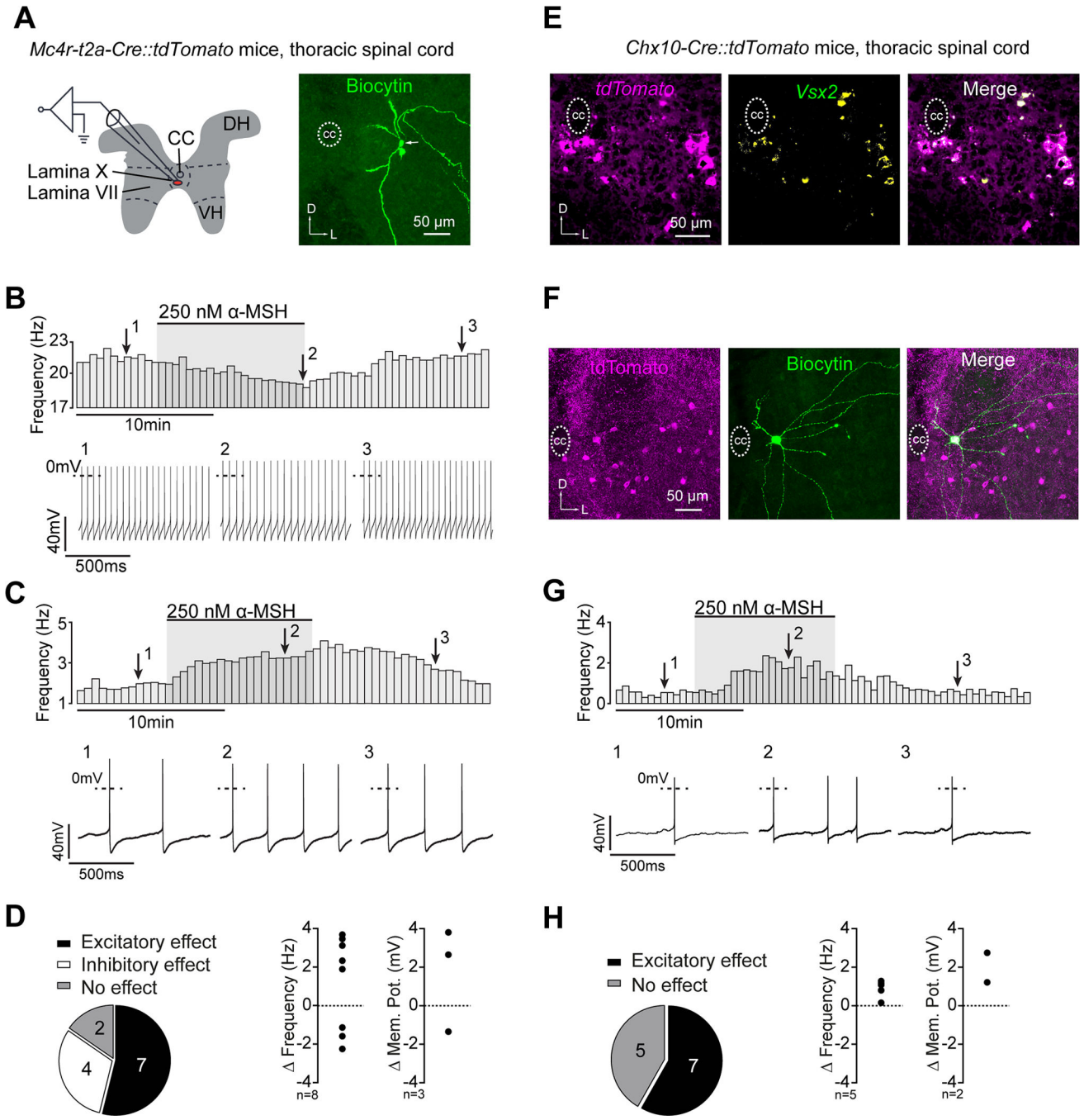

Figure 5: Mouse Mc4r and V2a neurons in spinal lamina X respond to α-MSH

(A) Schematic illustration of the electrophysiological recordings from lamina X *Mc4r::tdTomato* neurons (left) and Biocytin-streptavidin staining of a recorded *Mc4r::tdTomato* neuron (right). (B,C) Rate histograms with the respective original recordings showing the inhibitory (B) and excitatory (C) effects of α-MSH on action potential frequency of lamina X *Mc4r::tdTomato* neurons. (D) Distribution of excitatory, inhibitory, and no responses (left) and relative effects of α-MSH on action potential frequencies or membrane potentials of spontaneously active or silent *Mc4r::tdTomato*

neurons (right). (E) *V2a::tdTomato* neurons in *Chx10-Cre::tdTomato* mice as assessed by *Vsx2* in situ hybridization. (F) Biocytin-streptavidin staining of a recorded *V2a::tdTomato* neuron. (G) Rate histogram with the respective original recording showing the excitatory effect of α-MSH on a *V2a::tdTomato* neuron. (H) Distribution of excitatory responses (left) and relative effects of α-MSH on action potential frequencies or membrane potentials of spontaneously active or silent *V2a::tdTomato* neurons (right).

The α-MSH (250 nM) effect was measured 8–10 minutes after starting the bath application. Neurons were classified as responders when the change in action potential frequency or membrane potential was 3x larger than standard deviation. CC, central canal; DH, dorsal horn; VH, ventral horn.

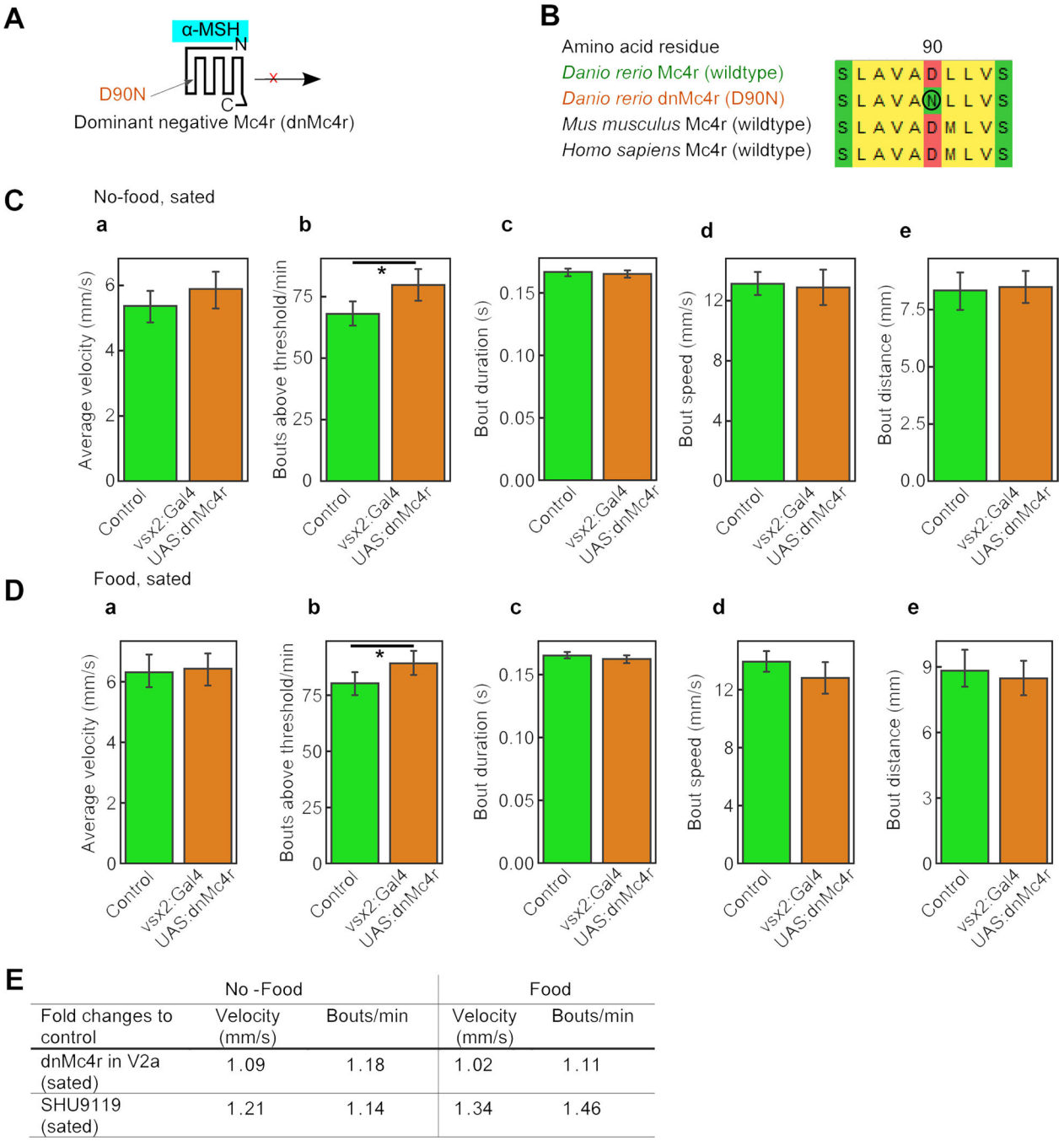

E

	No -Food		Food	
Fold changes to control	Velocity (mm/s)	Bouts/min	Velocity (mm/s)	Bouts/min
dnMc4r in V2a (sated)	1.09	1.18	1.02	1.11
SHU9119 (sated)	1.21	1.14	1.34	1.46

Figure 6. Disruption of Mc4r signaling in zebrafish V2A neurons modulates swimming behavior

(A) Schematic illustration of a dominant negative Mc4r with a D90N amino acid exchange. (B) Alignment indicates that Mc4r D90N mutation is localized in a highly conserved region. (C,D) Swimming behavior of *vsx2:Gal4FF; UAS:Mc4r(D90N)* double transgenic larvae and non-transgenic controls in absence of food (C) and with food (D) showed significant differences in swim bout frequencies (N = 8 animals, * = p<0.05, ** = p<0.01, error bars show confidence intervals). (E) Comparison of effects of V2a-specific dnMc4r /

Mc4r(D90N) (N=8) with the effects of the Mc4r antagonist SHU9119 (N=12; see Figure S4), each relative to the corresponding controls.